UC Merced

UC Merced Electronic Theses and Dissertations

Title

Saltwater Greenhouse Cooling System for Agricultural Drainage Treatment and Food Production

Permalink

https://escholarship.org/uc/item/5nb5d75s

Author

Brinkmann, Selina

Publication Date

2021

Peer reviewed|Thesis/dissertation

eScholarship.org Powered by the California Digital Library
University of California

UNIVERSITSY OF CALIFORNIA, MERCED

Saltwater Greenhouse Cooling System for Agricultural Drainage Treatment and Food Production

A Thesis submitted in partial satisfaction of the requirements for the degree of Master of Science

in

Mechanical Engineering

by

Selina Brinkmann

Committee in charge:

Professor James Palko
Professor Yanbao Ma
Professor Abel Chuang

Copyright

Selina Brinkmann, 2021

All right reserved

Signature Page

The Thesis of Selina Brinkmann is approved, and it is acceptable in quality and form for publication on microfilm and electronically

---

Professor James Palko, Supervisor and Chair

Professor Abel Chuang, Committee Member

Professor Yanbo Ma, Co-Supervisor and Committee Member

University of California, Merced

2021

I dedicate this thesis to …

… My family, who always believed in me.

… My sister and mother, who had to listen to endless phone calls.

… My brothers and father, who would listen if nobody else would pick up the phone.

… My friends, who kept in touch with me while living an ocean away. Shout out to Annika and Marvin!

… My new friends in Merced, who gave moral support and offered distraction.

… Tom, who always lifted me up.

… My grandmother, Oma Liesel, who sadly passed away but is always with me.

I appreciate you more than words can say. Thank you.

Contents

Abstract 13
1. Introduction 1
1.1 Motivation 1
1.2 Objective 1
1.3 Thesis Outline 1
2. Background 2
2.1 Central California and Agriculture 2
2.2 Irrigated Agriculture 2
2.3 Drainage Water Composition in San Joaquin Valley 2
2.4 Conventional Disposal of Drainage Water 3
2.5 Conventional Cooling Systems for Greenhouses 4
2.6 Spray Drying Technology 7
2.7 Particle Separation 8
2.8 State of the Art – Saline Water-Cooled Greenhouses 8
3. Conceptual Design 10
3.1 The Evaporation Chamber 11
3.1.1 Nozzle Selection and Specifications 11
3.1.2 Proposed Final Chamber Design 13
3.2 The Separation System 14
3.2.1 Active vs Passive Separation Systems 15
3.2.2 Proposed Final Separation Design 24
3.2.3 Salt Collection 25
3.3 Proposed Final System Design 26
4. System Modeling 27
4.1 Thermodynamic Model 27
4.2 Droplet Evaporation Time 29
4.3 Modeling results 31
4.3.1 System I 31
4.3.2 Full System 34
5. Experimental studies 42
5.1 Introduction of experiments 42

5.1.1 Experimental Design of Evaporation Chamber 42
5.1.2 Sensors, Data Collection and Processing 44
5.1.3 Evaporation with Distilled Water 46
5.1.4 Evaporation with NaCl 48
6. Overall System Function and Potential Improvements 51
6.1 Modelling 51
6.2 DI Water Test 51
6.3 NaCl Solution Test 53
7. Conclusion and Outlook 54
8. References 56

Nomenclature

Abbreviation

BGD	Billion Gallons per Day	
EAHES	Earth to Air Heat Exchanger	
EC	Electronic Conductivity	$\mu S/cm$
ECH	Evaporation Chamber	
EET	Estimated Evaporation Time	
ESP	Electrostatic Precipitator	
EVP	Evaporation Pads	
FS	Full Scale	
GH	Greenhouse	
GS	Greenhouse System	
MAF	Million acre-feet	
SS	Separation System	
SGS	Saltwater Greenhouse System	
SJV	San Joaquin Valley	
TDS	Total Dissolved Solids	mg/L
VPD	Vapor Pressure Deficit	

Greek Letters

γ	Constant required to calculate EET	67 Pa/K
Δ	Difference	-
η	Collection Efficiency	%
μ	Viscosity	kg/ms
ν	Kinematic Viscosity	m^2/s
ρ	Density	kg/m^3
ω	Absolute Humidity or humidity ratio	kg_w/kg_{da}

Symbols

a	Parameter required to calculate EET	m^2/s
A	Area/footprint	m^2
b	Parameter required to calculate EET	$m^{-1}s^{1/2}$
c_p	Specific heat capacity	kJ/kg/°C
C	Concertation	%
d	Diameter	µm or m
D	Diffusion Coefficient	-
da	Dry air	-
DF	Drag Force	N
G	Gravity Force	N
h	Enthalpy	J
H	Height	m
k	Shape constant	-
L	Length	m

$\dot{m}$	Mass Flow Rate	kg/s
M	Mass or Molecular Weight	kg
P	Pressure	kPa
q	Parameter required to calculate EET	$m^2s^{-1}K^{-1}$
$\dot{Q}$	Heat rate	kW/m2
R	Gas constant	8.3144 $J/mol^{-1}K^{-1}$
RH	Relative Humidity	%
s	Constant required to calculate EET	$-1.117x10^{-3}$ $ms^{-0.5}$
t	Time	sec
T	Temperature	°C or K
u	Velocity	m/s
V	Volume	m^3
W	Width	m
x	Ratio of chamber residence time to particle settling time	-
X	Size Classification	µm

Indices

1	Inlet Evaporation Chamber	
2	Outlet Evaporation Chamber/Inlet Greenhouse	
3	Outlet Greenhouse	
a	Air	
amb	Ambient	
ap	Pressurized Air	
atm	Atmosphere	
cor	Corrected	
C	Cut-Size	
d	Droplet	
f	Film	
g	Gas or saturation vapor	
GH	Greenhouse	
L	Liquid	
max	Maximum	
o	Initial	
P	Particle	
r	Residence	
s	Settling	
T	Total	
v	Air vVapor	
wetb	Wetbulb	
W	Water	

List of Figure

Figure 1: Schematic diagram of spray-drying process. 8

Figure 2: Conceptual design of proposed system including all necessary components. 10

Figure 3: Schematic drawing of the working principles of an ultrasonic nozzle . 12

Figure 4: BETE XA-PR 050 Dual Fluid Nozzle with internal mixing. 13

Figure 5: Evaporation Chamber Design Based on Nozzle choice and alignment. 14

Figure 6: Particles of cut-size are at mechanical equilibrium (drag force DF = gravity force G). Coarse particles move downward while fine particles follow air stream upward. 16

Figure 7: Simple settling chamber. 17

Figure 8: Settling chamber dimensions for a simple settling chamber. 19

Figure 9: Basic Louver-Type Separator 20

Figure 10: Modified louver separator schematic with dust container and simplified particle trajectory 20

Figure 11: Particle separation using electrostatic precipitator. 21

Figure 12: Basic bag filter separation system 23

Figure 13: Centrifugal separator and operating principles 23

Figure 14: a) Schematic of separation system with the two separation mechanisms chosen, louver-type and electrostatic precipitator. 25

Figure 15: Louver Type Separator. 25

Figure 16: Final system design including all components. 26

Figure 17: Schematic of heat transfer model including relevant variables. 28

Figure 18: Outlet temperature T_2 and humidity ratio w_2 versus air flow rate $\dot{m}_a$ for different inlet temperatures. 32

Figure 19: Outlet temperature T_2 and absolute humidity w_2 versus air flow rate for different inlet relative humidity's. 33

Figure 20: VPD_{GH}, T_{GH}, RH_{GH} versus air flowrate for T_1 = 30 °C, RH_1 = 15 % and Q_{Sun} = 0.5 kW/m^2. 36

Figure 21: VPD_{GH}, T_{GH}, RH_{GH} versus air flowrate for T_1 = 33 °C, RH_1 = 15 % and Q_{Sun} = 0.5 kW/m^2. 37

Figure 22: VPD_{GH}, T_{GH}, RH_{GH} versus air flowrate for T_1 = 30 °C, RH_1 = 15 % and Q_{Sun} = 0.75 kW/m^2. 38

Figure 23: VPD_{GH}, T_{GH}, RH_{GH} versus air flowrate for T_1 = 33 °C, RH_1 = 15 % and Q_{Sun} = 0.75 kW/m^2. 39

Figure 24: Estimated Evaporation Time (EET) for water droplet at RH_1 = 15 %, Q_{Sun} = 0.5 kW/m^2 and a) T_1 = 30 °C and b) T_1 = 33 °C. 40

Figure 25: EET for water droplet at T_1 = 30 °C, Q_{Sun} = 0.5 kW/m^2 and a) RH_1 = 15 % and b) RH_1 = 20 %. 40

Figure 26: EC footprint for 1 m^2 of greenhouse with chamber height H_{ECH} = 1.5 m at VPD_{GH} = 1.0 kPa, RH_1 = 15 %, Q_{Sun} = 0.5 kW/m^2 and a) T_1 = 30 °C and b) T_1 = 33 °C. 41

Figure 27: EC footprint for 1 m^2 of greenhouse with VPD_{GH} = 1.0 kPa, RH_1 = 15 %, Q_{Sun} = 0.5 kW/m^2, T_1 = 30 °C and a) H_{ECH} = 1.5 m and b) H_{ECH} = 2.5 m. 41

Figure 28: Evaporation chamber for experimental tests. 43

Figure 29: Additional air flow measurements. 45

Figure 30: Data for distilled water evaporation test run. 46

Figure 31: Comparison of Model and Experimental Data for Evaporation Chamber with Clean Water. 47

Figure 32: Comparison of Model and Experimental Data for Evaporation Chamber with 1% NaCl Solution. 49

Figure 33: Salt Recovery. 50

List of Tables

Table 1: Average of minerals and trace rlements found in the Northern, Central and Southern Area Drains. 3

Table 2: Particle classification based on size. 15

Table 3: Cut-Size of particles in m based on final system. 17

Table 4: Footprint of simple settling chamber for particle size 5 μm, 7.5 μm and 10 μm and efficiency of 50%, 75% and 90% at an air flow rate of 0.07 m^3/s 19

Table 5: Separation Systems Sorted by Cut Size Xc, Gas Velocity, Pressure Drop, Energy Dissipation, Operating Temperature and Required Operating Space. 24

Table 6: Sensor Specification 44

Table 7: Operating conditions during water evaporation test.. 47

Table 8: Change in VPD_{GH} and T_{GH} over measured inlet data and range of Q_{Sun}. 48

Table 9: Operating Conditions during 1% (w/w) NaCl Solution Evaporation Test. 49

Acknowledgments Page

Selina Brinkmann (SB) acknowledges the following grants to make the thesis possible:

The work was supported by the National Science Foundation (INFEWS:T2), Award Number 1856112.

SB would also like to thank the German Academic Exchange Program (DAAD) for supporting her studies in the US.

SB would also like to thank the Friedrich-Naumann Stiftung for Freedom (FNF) for supporting her through her undergraduate studies and her endeavor at UC Merced.

Last but not least, SB wants to express her gratitude towards Professor James Palko (JB) for being an attentive and supportive supervisor. His support and input were helpful throughout the theoretical and experimental parts of the project. Without JP and the time in his lab, SB would not have been courageous enough to apply for her PhD at Oxford University. Thank you!

Abstract

Freshwater consumption in greenhouse (GH) cooling is a major concern for agriculture in Central California. A spray drying system to cool greenhouses is studied. Such a system can intake drainage water from agricultural fields thus lowering freshwater usage. As an additional benefit of the system, minerals dissolved in the wastewater can be collected in solid form, which would reduce the need for expensive wastewater treatments to meet environmental standards. The system consists of an evaporation chamber (ECH) and a precipitate separation system (PSS). Water droplets ranging from 15 to 30 μm are sprayed into the chamber. Hot outside air moved by fans into the ECH evaporates the water, thus, decreasing the temperature while increasing humidity. The cold and moist air then transports the solid precipitate particles to the PSS. There, a louver-type separator takes advantage of the inertia of the solids. Unable to change direction as fast as the airflow, the particles accumulate in a dust chamber. At the system output, clean cold air is released into the GH to lower the inside temperature and provide an agreeable habitat for plants. The feasibility of the ECH is assessed via thermodynamic and kinetic models and experimental characterization of a prototype chamber in the laboratory. Measured and predicted values for outlet temperature and humidity differ by 2 to 11 %, which is within the combined uncertainty of the measurements and model. A prototype louver-type separator recovers 35 % of the total supplied solids from 1% NaCl feed solution. Given representative conditions, the chamber footprint required to cool a 100 m^2 GH ranges from 4 to 10 m^2.

1. Introduction

1.1 Motivation

California produces a large percentage of the fruits and vegetables consumed in the United States of America and is the leading state in crop cash receipts with a revenue of approximately $50 billion most of which is earned in the Central Valley [1]. Produce grown in California includes but is not limited to nuts, citrus fruits and berries. Currently, 77,100 farmers are operating in California and entrusted to meet 50% of the country's fruit and nut demands while supplying 1/3 of the nation's vegetables [2]. As a side effect of heavy agriculture, irrigation return-flows are salt and particle-laden [3]. This leads to an increase of salt accumulation in soil and ground water which decreases crop productivity and threatens the sustainability of farming lands in California [4]. A cost-efficient greenhouse system (GS) running on drainage water would reduce salinization while decreasing freshwater consumption. In addition, it would also ease the financial burden of farmers in the Central Valley as water bills could be cut down and salt collection simplified making it easier to meet water standards.

1.2 Objective

The objective of this work is to develop a cost-effective evaporator using agricultural drainage water to cool down a saltwater greenhouse system (SGS) with zero-discharge, recovery of minerals, and minimized environmental impact.

1.3 Thesis Outline

The thesis is split into seven chapters. The first chapter introduces the main motivation behind the project and the final objective. Chapter 2 provides background on the problem and technology underlying the proposed solution. Chapter 2 gives an insight into the relevance of the San Joaquin Valley and the struggles of increasing soill salinity. It discusses advantages and drawbacks of conventional salt disposal methods and greenhouse cooling. The chapter also describes how salt drying technology works and how solid particles can be separated from air. It ends with a short overview of salt-water cooled greenhouses currenlty in operation and their differences to with the current research. Chapter 3 shows the conceptual design of the proposed system and its individual elements. The following chapter introdues the thermodynamic and kinetic models used to estimate evaporation rate, salt collection and chamber size. It also discusses the influence of various inlet conditions on the greenhouses temperature and relative humidity. Chapter 5 then deals with the actual experimental setup used and the test results for deionized water and 1 % NaCl solution. Chapter 6 discusses the overall behavior of the system and provides potential avenues for improvement. The thesis finishes with a short conclusion and brief outlook on testing outside laboratory conditions.

2. Background

2.1 Central California and Agriculture

The Central Valley of California has been crucial to American agriculture since the mid-1800s when it was known for its grain operations, second only to Minnesota. However, due to monocrop farming and lack of fertilizer use among other factors, California saw a steady decrease in grain quality and production by the 1890s which led to a shift in agriculture towards fruit cultivation. As a result of the change to intensive farming, irrigation needs increased steadily from 1 to 16% in the span of 40 years [5]. Today, the Central Valley produces a quarter of the Nation's food using 75% of the 7.9 million acres of irrigated acres across California [6], [7]. For example, all of the Nation's almonds, figs, olives and most of the Nation's citrus fruits are cultivated in California [1].

2.2 Irrigated Agriculture

Irrigated agriculture refers to the acreage where crop production is independent of rain. Water is supplied to the fields through pipes, sprinklers and streams which are fed by groundwater wells, surface water and off-farm water [7]. Both M. Maupin et al. [8] and [9] agree that the majority of California's water use goes towards irrigation. Their estimates vary between 26 million acre-feet (MAF) and 33 MAF which is equivalent to 23 to 29 billion gallons per day (BGD) [10]. Considering that the Central Valley uses 75% of the irrigated acres in California to grow their crop, 17 to 22 BGD are needed to sustain their agriculture. However, using high amounts of water for irrigation purposes has multiple side effects such as contaminating groundwater bodies through pesticides and other minerals, salinization of soil and depletion of freshwater sources. The research focus of this thesis is, to replace freshwater usage in greenhouses by drainage water to simultaneously simplify the disposal of wastewater, decrease salinization and reduce contamination.

2.3 Drainage Water Composition in San Joaquin Valley

The composition of drainage water depends on multiple factors. Four of them, the salinity of the water supply, the salinity of the soil, the pesticides used, and the drainage type will be further assessed in this section. In **Table 1**, a detailed composition of the drainage water in the Central Valley is given, based on the San Joaquin Valley (SJV) Drainage Monitoring Program [11]. However, most of the water supplied to agriculture in the Central Valley exceeds the general salinity level of 700 μS/cm measured in electric conductivity (EC) recommended by R.S. Ayers and D. W. Wescot [12]. The salts are byproducts of weathering of rock, soil and other minerals and remain behind once the water is consumed by the crops or evaporated [12]. As a consequence, agriculture had to adapt by using less selective crops or by increasing their water usage to compensate for the higher salinity level, both non-sustainable choices [13]. However, if supplying extra water to leach the salt from the soil is not possible, salinization occurs which reduces future crop yields, and the drainage water has an increased salinity level.

The west side of the Central Valley has naturally saline soil, which can be traced back to the Mesozoic and Tertiary age. The sediments contained within those rock layers are rich in salts, boron and selenium (Se) which increase the salinity level of drainage water and make further treatment vital, as Se is toxic to wildlife [14], [15]. See **Table 1** for actual amount of minerals and elements in the San Joaquin Valley which confirm that the SJV is a problem area, with the EC being ten times the recommended value. Even though pesticides can be found in elevated concentrations in drainage water, good monitoring and proper management reduce the risk associated with them. In addition, slight adjustment to the administration or farming practice can ensure that spikes in concentration are limited to surface runoff and short periods of time. Subsurface drainage water is less likely to have high concentrations or pesticides due to the filtering ability of the soil. An average amount of pesticide in subsurface drainage water is less than 0.1% of that in the water supplied [16].

Table 1: Average of minerals and trace elements found in the Northern, Central and Southern Area Drains. Adapted from SJV Drainage Monitoring Program. Pesticides are not listed as none were found to be above drinking water standards [11].

Minerals and Elements	**San Joaquin Valley**
	mg/L
Boron	12
Calcium	330
Chloride	1109
Magnesium	192
Nitrate	121
Selenium	0.09
Sodium	1737
Sulfate	3402
Total Dissolved Solids (TDS)	6912
EC (μS/cm)	8135

2.4 Conventional Disposal of Drainage Water

Currently there are five major ways to dispose of drainage water. It can be disposed in natural water systems such as lakes and rivers; it can be used as part of land retirement; it can be placed in evaporation ponds for disposal, injected into a deep well or reused in irrigation. There a multiple advantages and disadvantages to each of those procedures and the following text will discuss them [16].

If drainage water is returned to a natural hydrological system, the amount that can be disposed of depends on the hydrology and water quality of the system. A lake for instance needs a high enough outlet flow to prevent the accumulation of contaminants. A river can tolerate higher contamination, but further downstream usages must be considered. If the water is used for drinking purposes, safety standards need to be adhered to [16].

Land retirement is a term used in agriculture which refers to a parcel of land no longer used for crop production due to salinization or unreasonably high levels of selenium. The owner is compensated to stop farming this particular lot but exceptions are made if rain water is used as a method of irrigation [17]. However, this drainage solution requires substantial amounts of land and long-term impacts on the soil have to be considered [16]. If natural water systems are too far from the irrigated land, drainage water is often disposed of in basins. There, evaporation ponds are built by moving soil from the basin center outwards to construct embankments. To avoid seepage, additional drain systems are incorporated around the perimeter of the pond. In most cases the shallow groundwater in the basin will have a degraded water quality. In addition, traces of Se in the drainage water can accumulate until they reach a critical stage which has proven to be toxic to wildlife - water birds in particular are drawn to the open water bodies [18].

California also tried to adapt deep well injection technology, already used for brine disposal by oil and gas companies, to drainage water. In deep well injection, the brine is disposed in reservoirs below the deepest source of freshwater. Those reservoirs contain concentrated saltwater and are made from porous or permeable rock. However, a prototype in the San Joaquin Valley was only able to dispose of 20% of the intended rate and the project was discontinued [16].

Another popular method to dispose of drainage water is to use it to irrigate less selective crops. In general, those plants have a higher salt-tolerance and are low-maintenance to grow. However, the sustainability is questionable as each consecutive reuse of drainage water increases the salinity of the runoff water and the crops used in the next cycle must be even more salt-tolerant. The economic feasibility plays a major role in the selection of this disposal type [14].

All these conventional disposal forms have something in common, they are costly in either monetary or resource terms. Either water needs to be transported long distances, fertile land is turned into wasteland, the method is not sustainable over a long period of time or crop yields drop, which lowers the yearly revenue. If a system is developed which allows agriculture to reuse the water on-site while simultaneously removing the contaminants and salt, freshwater usage would decrease. This would lower water bills, leave more freshwater to compensate during droughts while also eliminating the need for expensive disposal.

One possible system to take advantage of the drainage water is to use it in greenhouse cooling. Especially in arid regions, greenhouses require a lot of freshwater to keep the interior climate suitable for plant growth. Replacing the freshwater with drainage water will combine the advantages mentioned earlier, e.g. less land retirement or disposal cost along with reduction in freshwater usage required by most conventional cooling systems.

2.5 Conventional Cooling Systems for Greenhouses

Greenhouses are used in agriculture to create a pleasant growing climate for plants. In contrast to open field cultivation, farmers can control the amount of light received by the plants, manipulate the amount of water delivered to the plants and control the climate. The latter is crucial in California as the daily average temperature in the summer months

ranges between 70°F and 76°F but high temperatures can reach 120°F in the more arid regions, while precipitation is low, barely reaching 0.3 inches in June [1]. To reduce the temperature inside a GH in the summer months, various cooling systems can be used. The most common ones are introduced in the following sections including the ones that require freshwater input.

Natural Ventilation

One way to reduce the air temperature in a greenhouse is by adding or improving ventilation. Openings on the side and roof allow natural convection, taking advantage of the density difference between hot and cold air. The colder outside air moves in, while the warmer air is pushed through the roof opening. Wind speeds of less than 3 mph already contribute to ventilation [19]. However, this method is more likely used in regions with milder climates, as the minimum inside temperature is limited by the outside temperature. A drop of 2 to 3 °C is, generally, the most achieved by natural ventilation, which is not enough to make a greenhouse with 42 °C interior temperature a place suitable for growing plants [20].

Forced Ventilation

In comparison to natural ventilation, fans are employed to increase the air exchange rate and lower the inside temperature to create a crop friendly environment. However, a study conducted by D. H. Willits proved that beyond an airflow of 0.05 $m^3 m^{-2} s^{-1}$, no advantage could be seen unless the fan was combined with an evaporative pad [21]. Thus, while a steeper temperature drop can be achieved, it is not enough to rely on such a system during the summer months in a hot climate [20].

Shading

Another method to reduce the inside temperature is to minimize the amount of solar radiation received by the GH. This can be done by using plastic nets or reflector sheets, applying whitewash or running a thin water film over the roof. Excluding the water film, all those approaches have one thing in common: they are inexpensive as they are easy to setup and to maintain. As a side benefit to cooling the greenhouse, shading can improve the light distribution and create a more uniform temperature and relative humidity. As a result, plant quality increases while plant stress is reduced [22]. However, even though shading decreases the amount of solar radiation received by the GH, the maximum temperature drop in hot climates is limited due to higher solar intensities. Nevertheless, in contrast to natural ventilation, a temperature drop of 4 to 6 °C can be achieved [20].

Geothermal Cooling – Earth Tubes

Greenhouses can be cooled by taking advantage of lower temperatures in soil. Below the surface, the earth has a constant temperature of 26 to 28 °C [20]. By moving hot air through pipes buried up to 4 m deep, the exit air reduces greenhouse temperatures by

5 to 6 °C in summer. As a side benefit, earth to air heat exchangers (EAHES) increase the GH temperatures in winter months which makes year-round farming easier [23]. However, EAHES have two major drawbacks - capital cost is high, due to the construction work required by the system, and leakage or deterioration of the pipes is hard to detect once the system is fully installed [20].

Evaporative Cooling

Besides ventilation, evaporative cooling is one of the most well-known methods in greenhouse cooling. It can be divided into three major subgroups: fan-pad system, fog/mist system and roof evaporation [20]. Evaporative cooling works on the following principle: once water is introduced to hot air; it will turn into vapor if enough energy is available. In greenhouses this energy is the excessive heat. As a result, the temperature drops.

Fan-Pad-System

In a fan-pad-system, a pad is mounted at the entrance of the greenhouse while a fan is installed on the opposite end. Using a distribution pipe, a constant water stream is created which wets the pad material evenly. As the air is pulled towards the fans and through the pad, its temperature drops while humidity increases. However, evaporative cooling pads (ECPs) have multiple drawbacks. If the supplemented water is rich in impurities, the pads can clog which reduces the efficiency. As a side effect, algae growth also increases, which reduces the lifetime of the system. Thus, systems with ECPs do not run on drainage water due to its high salt content but rather on freshwater, which increases cost especially in arid regions. In addition, the pads need to be uniform to ensure that air travels through the whole pad and not sections with holes or other irregularities. If air would move through a hole, it would not come in contact with water and provide less cooling [24]. However, if a fan-pad-system is used alongside shading, a temperature drop of up to 12 °C can be achieved [20].

Fog/mist system

Another way to take advantage of evaporative cooling is by spraying small droplets of water into the air as their increased surface area aids evaporation. Nozzles are spread out through the greenhouse to create a more uniform temperature and humidity distribution in comparison to a fan-pad system where there is a gradient in temperature (cool close to the pad and hot near the fan) [20]. Mist or fog systems achieve temperature drops of up to 8 °C, but they cannot be used with degraded water as they traditionally spray into the air above the plants, which cannot tolerate the precipitate left after evaporation. In addition, the high levels of humidity achieved by a fog or mist system can make the crop more vulnerable to diseases as microorganisms thrive in such an environment [20].

Roof Evaporation

Here, water is sprinkled onto the roof in a thin layer to increase the surface area and the evaporation rate. As a result, the GH internal air temperature is reduced up to 6 °C and solar radiation transmissivity decreases by 6 %. However, both values can be increased if some form of shading is used. Nevertheless, roof evaporation is less effective than the other two evaporative cooling systems as the internal air does not get in direct contact with the water. This can be a benefit in some climates as the humidity is not increased and the corresponding growth of microorganisms is not promoted [20].

Conclusion

While shading and natural ventilation require little to no additional resources and energy input, the temperature drop achievable is small. To obtain a bigger temperature drop and reduce operational and capital cost alike, an alternative system is needed that takes advantage of the free energy and resources provided by the surroundings, i.e. hot air and drainage water. Considering the tendency of clogging while operating fan-pad-systems with saltwater, fog/mist systems achieve a similar temperature reduction through evaporation and can be run with drainage water, provided the precipitate remaining can be kept away from the plants. To collect the elements and minerals suspended in the drainage water and prevent them from contaminating the plants in the greenhouse upon cooling, spray drying technology will be used in this research. As a result, a cold air stream devoid of any solid particles will enter the greenhouse.

2.6 Spray Drying Technology

Spray drying is used to extract solids from a liquid through evaporation and has been around since the late 1800s. Applications include the dairy and chemical industry where it is used due to its efficiency and reliability [25].

Evaporation describes the phase transition when liquid molecules receive enough energy (i.e. from heat) to break their intermolecular attraction and become part of their gaseous surroundings. As an alternative to supplementing heat to increase the evaporation rate, the ambient pressure can be reduced [26]. Increasing the surface area of the liquid further aids the evaporation process, hence most spray drying processes rely on atomization to create small droplets. Those atomizers can be divided into the following categories based on their energy usage: rotary, pneumatic, pressure and ultrasonic. Some of the atomizers utilize multiple energy sources, and their usage can be limited by the feed stream characteristics or desired droplet size [25]. The following schematic, **Figure 1**, depicts a conventional spray drying process.

The liquid solution is fed to the nozzle at the top of the evaporation chamber. Here atomization occurs using either centrifugal, kinetic, pressure or acoustic energy. The advantages and disadvantages of the different atomizers are discussed in the conceptual design of the evaporation chamber. Once the droplets encounter the hot gas, they evaporate and reduce the gas temperature while simultaneously increasing the humidity. The particles

suspended in the colder gas are transported to a separation system such as a cyclone separator or electrostatic precipitator.

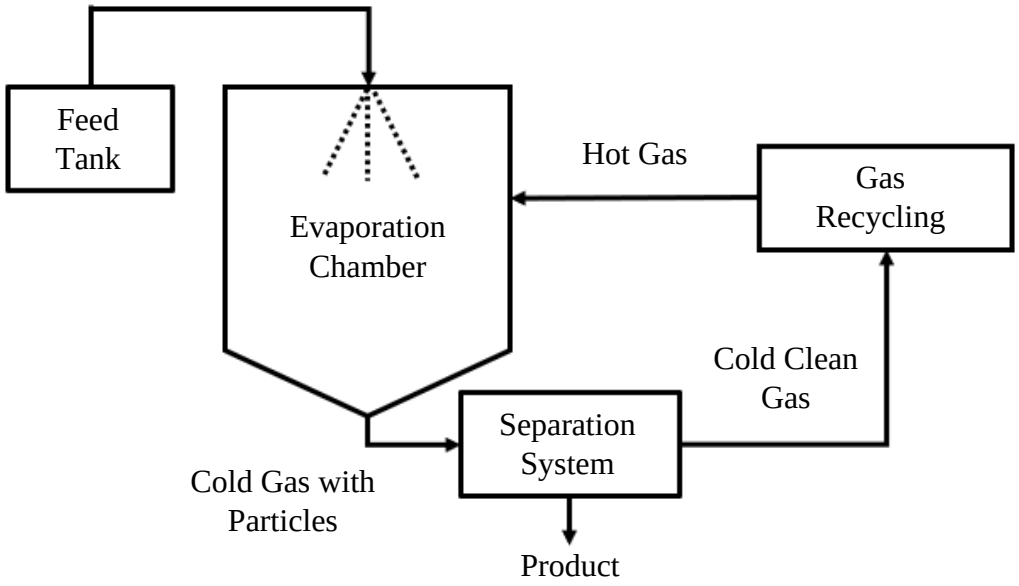


Figure 1: Schematic diagram of spray-drying process. Liquid is supplied to the evaporation chamber using a feed tank and nozzle. Then, particles are separated from the cold gas before the fluid is reheated and resupplied to the chamber.

2.7 Particle Separation

As previously mentioned, depositing minerals and other solutes in large quantities on the plants can be harmful. In addition, greenhouse workers could come into contact with toxic aerosols and suffer health issues. Thus, prior to entering the greenhouse, the cold air stream laden with particles needs to be cleaned. This allows the operation of the greenhouse on drainage water rather than costly freshwater. It also reduces the disposal cost of contaminated water, as the minerals are recovered dry and can be disposed of at landfills. Separation methods using gas as a medium can be divided into two major subgroups: passive and active. The former takes advantage of gravity and inertia of the solid particles while the latter requires energy input. As the design and efficiency vary heavily between different separation methods, their advantages and limitations are addressed in the conceptual design section of this thesis.

2.8 State of the Art – Saline Water-Cooled Greenhouses

As discussed, there are multiple ways to cool greenhouses. Most of them are restricted to run on freshwater due to fouling issues, e.g. fan-pad systems, or due to particle deposition in the greenhouse, e.g. fog systems inside greenhouses. This is not a major concern if the greenhouses are located in mild to cold climates, but it becomes troublesome

if the greenhouse is built in arid regions or far from clean water sources. Brackish water and groundwater with high salinity render common cooling systems useless [27]. Literature shows that the operation of greenhouses with salt or drainage water has been a recent focus in agricultural research due to continuously high food demand and the earth population growing.

T. Akinaga et al. [28] showed that the excess water in brine can successfully be used for cooling and salt can be collected. However, their system relies on the usage of evaporation ponds after the supplied brine has been recirculated multiple times to increase the salt content rather than full evaporation of the water in the brine for cooling. This increases the footprint of the system and is more applicable for a collaboration between desalination plants and agriculture rather than standalone farmers, e.g. in the California Central Valley.

The system designed by K. Lüchow and C. von Zabelitz [27] on the other hand, appears to follow a similar strategy as the proposed system – low cost of investment, low energy consumption and low maintenance. In addition, the system also utilizes nozzles rather than an evaporation pad system as used by T.Akinaga [29]. Once more, however, full evaporation is not the ultimate goal but rather a steady increase in salt concentration of the supply water. The system in [27] also has an objective to operate with low water consumption contrary to the proposed design were salt collection is the primary goal, followed by replacing freshwater usage for cooling purposes. Similar approaches can be found in [30], [31] and [32].

In [29], the saline water was used for evaporation via EVPs. The authors mentioned salt accumulating in the supply tank but made no further comment about the brine disposal. Fouling of the EVPs is prevented by running high amounts of saline water through them. Fresh water collection through condensation was the operation goal. A review in [30] offers an overview of advances in seawater greenhouses in the past years. Once again, the main goal is the collection of fresh water and cooling of the greenhouse rather than removing the salt and preventing it from re-entering the water cycle by disposing of it in dry form.

Reference [31] uses a thin water film rather than EVPs to achieve evaporation. Just like the other systems, a brine rather than solid salt particles needs to be disposed of. Using a solar distiller in conjunction with solar ponds allows the authors to store thermal energy that can be used to produce cold water in a solar absorption unit. However, the paper does not mention actual reuse of the brine or testing the suggested setup.

The system considered in this work differs from previous studies in the capability of full water evaporation in combination with maximum drainage water disposal and dry salt accumulation in a separator system. This reduces the complexity and size of the system as the setup consist of only four major components: the evaporation chamber (ECH), the separation chamber, a fan and the greenhouse. See the following **Chapter 3** and **Figure 2**.

3. Conceptual Design

The following chapter addresses the different components and factors required to design the degraded water-cooling system. See

Figure 2 for the overall system architecture. To ensure affordability of the system and easy installation for pre-existing greenhouses, the cooling and separation processes take place outside the greenhouse. Using a fan, the ambient air is pulled into the evaporation chamber (ECH). Drainage water is atomized using a nozzle and evaporates upon contact with the warm air. Humid and cold air laden with particles leaves the chamber and enters the separation system. Here, the particles are separated from the air. Cold and clean air then enters the greenhouse through ducts replacing conventional cooling systems operating on freshwater. The sun slowly reheats the air in the greenhouse. The air is released less humid and warmer into the surroundings while the particles are disposed of in solid form.

As the size of the chamber depends on the evaporation rate of the droplets, choosing the correct nozzle is particularly crucial. **Chapter 3.1** will discuss the advantages and disadvantages of each type before showing the one used in experiments. Knowing the nozzles and droplet size, enables one to choose a separation system, as the solid particle size can be predicted.

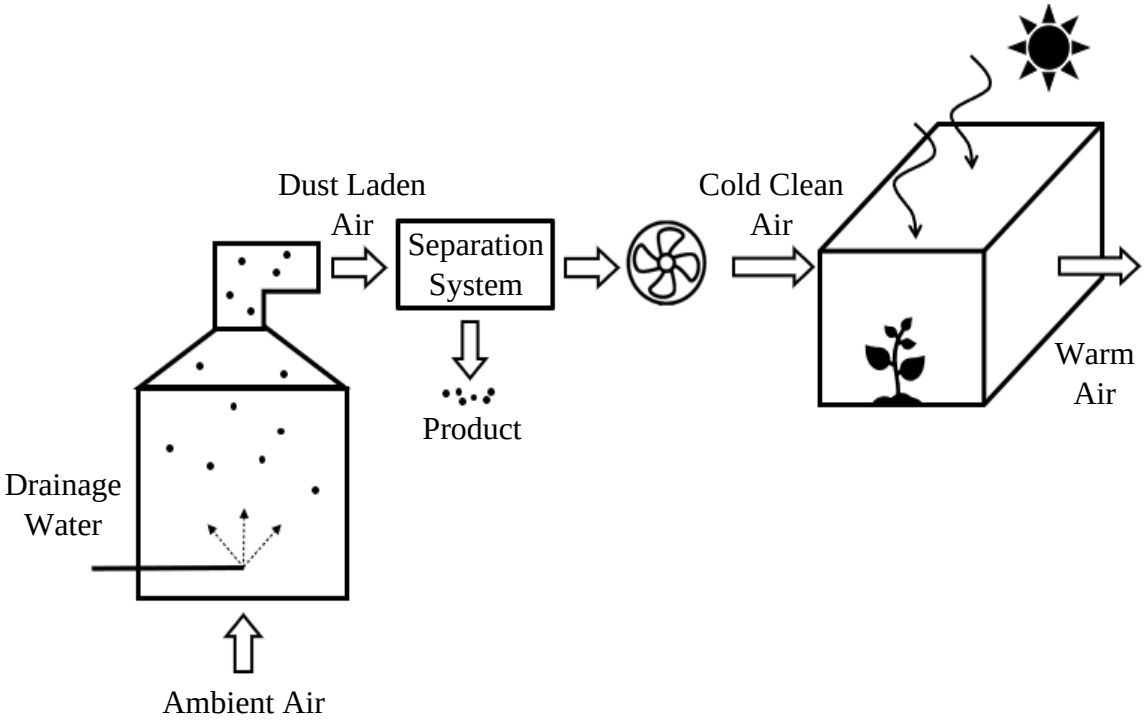


Figure 2: Conceptual design of the proposed system including all necessary components.

3.1 The Evaporation Chamber

To be able to capture the particles suspended in the drainage water, full evaporation of the water droplets is required. This is only possible if they are given enough time in the warm air stream. However, the time needed can be reduced if the surface area to volume ratio is increased. The smaller the droplet, the bigger the ratio and the shorter the evaporation time. Thus, choosing the correct nozzle is an important step in the design process as the system should be as small as possible while still accomplishing separation and cooling.

3.1.1 Nozzle Selection and Specifications

As mentioned in Chapter 3.6, atomizer selection depends on multiple factors: the required droplet size, the feed stream characteristics and the energy resources available for operation. However, the droplet size is the most important factor, as small droplets allow rapid and complete evaporation in a reasonably sized chamber. The following paragraphs discuss the advantages and disadvantages of the individual nozzles and allow one to understand why certain types were preferred to others in the experiment. In general, one can say: the higher the feed rate, the bigger the spray angle. Similarly, the higher the feed pressure, the smaller the droplets. Only two-fluid nozzles behave differently, as a higher feed rate at the same gas flowrate creates bigger droplets while an increase in gas flowrate reduces the droplet size [26].

Rotary Nozzle

Here, atomization is achieved through centrifugal energy. The liquid solution is poured on top of a rotating surface - either a disk or wheel, which is moving at speeds between 3,000 to 50,000 rpm. At the edge of the surface, the liquid solution is forced to break into droplets. A major advantage for this approach is that rotary nozzles, contrary to other spray heads, do not clog and are able to create droplets of uniform size [26], [25]. However, their capital cost is higher, and the chamber system is generally wider than in other atomizing devices [33].

Twin-Fluid Nozzle

In two-fluid nozzles, a gas stream at high velocity is used to atomize the liquid solution. The fluids can mix either internally or externally. The prior allows for smaller droplet size and is more efficient. As both streams can be adjusted separately, it is possible to create fine droplets at low liquid speeds. However, these types of nozzles can clog depending on the particles suspended in the liquid solution and fairly large amounts of air might be needed to achieve the desired droplet size [25].

Pressure Nozzle

Also known as hydraulic nozzles, produce droplets by forcing a pressurized liquid solution through a shaped chamber and opening. There, the liquid velocity increases and breaks the stream into individual droplets. Pressure nozzles can be found everywhere from household to industrial application. Similar to twin-fluid nozzles, pressure nozzles can clog if the liquid solution is not chosen according to the atomizer design. They are less complex than both rotary and twin-fluid nozzles, and most of the time, their operational cost and energy consumption is lower [34]. As an increase in hydraulic pressure is accompanied by an increase in flow rate as well as a decrease in droplet size, it is crucial to consider flow requirements and the size of the drying chamber [25], [26].

Ultrasonic Nozzle

These nozzles are mostly used in the biomedical or electronic industry due to their fine droplets and low flow velocity. Vibrations are created with a piezoceramic element that converts electric energy to mechanical energy. Compressed air or a pressurized liquid are not needed. Instead, the liquid solution inserted into the nozzle develops capillary waves. **Figure 3** shows a schematic drawing of an ultrasonic nozzle to illustrate the inner workings. With enough energy, the capillary waves will become unstable and break into smaller drops. Additional elements in the nozzle can amplify the capillary waves, thus reducing the energy needed. However, ultrasonic nozzles are still in the development and research phase. As such, their throughput is much lower in comparison to the other nozzles introduced [25], [26].

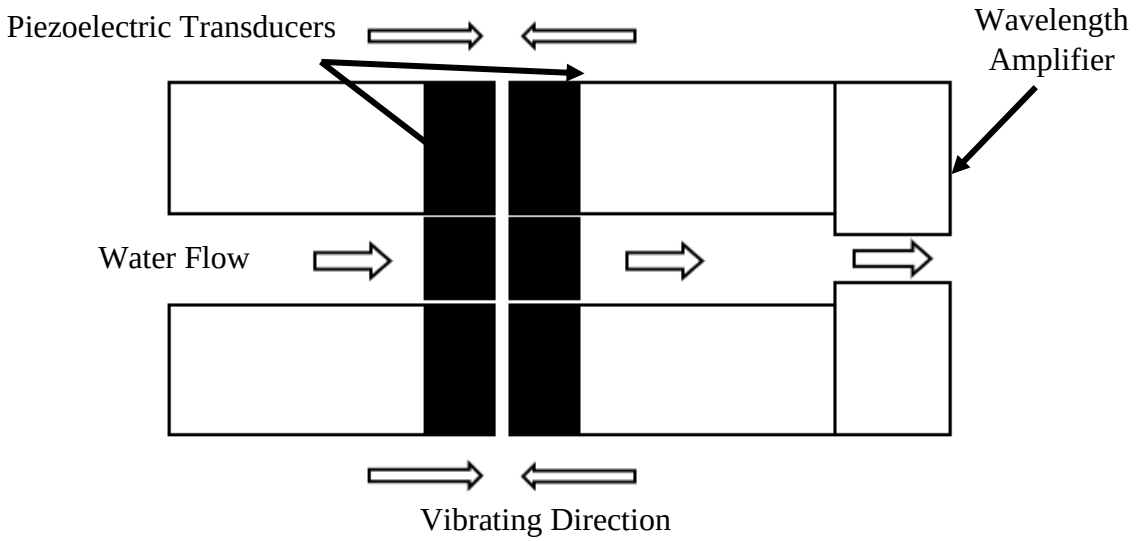


Figure 3: Schematic drawing of the working principles of an ultrasonic nozzle by N. Ashgriz [26]

Nozzle Selection for System

As fine droplets are required by the system, and the temperature at the inlet depends on the ambient air outside, both the rotary nozzle and the twin-fluid nozzle were considered. The latter having the advantage over a plain pressure nozzle that the water flow is adjustable while maintaining small droplets by supplementing pressurized air. This is helpful especially during days with big temperature range where consistent droplet size is required over a wide range of water flow rate. The cost of rotary nozzles at small quantities influenced the decision in favor of the twin-fluid nozzle for the first stages of the project. If the system is successful in cooling a greenhouse and collecting salt simultaneously, rotary nozzles may be used in the final design as they cannot clog and will keep operation cost low.

Chosen Nozzle for Experiments

The chosen nozzle XA-PR 050 is manufactured by BETE and can be seen in the following **Figure 4**. It is an internal mix, pressure-fed nozzle with a narrow spray angle of 12° to 22°. Operated between 6 to 9 PSI Liquid and 9 to 12 PSI Air, the nozzle produces a fine mist with droplet size ranging from 25 to 30 µm at a water flow rate between 22 mL/min to 26 mL/min. As the chosen operating pressures are outside the range provided in the specification sheet, BETE and their application engineer, Everest Peacock, provided the expected droplet size. Due to the narrow angle, the nozzle sprays up to 7 ft. This needs to be taken into consideration for the proposed chamber design.

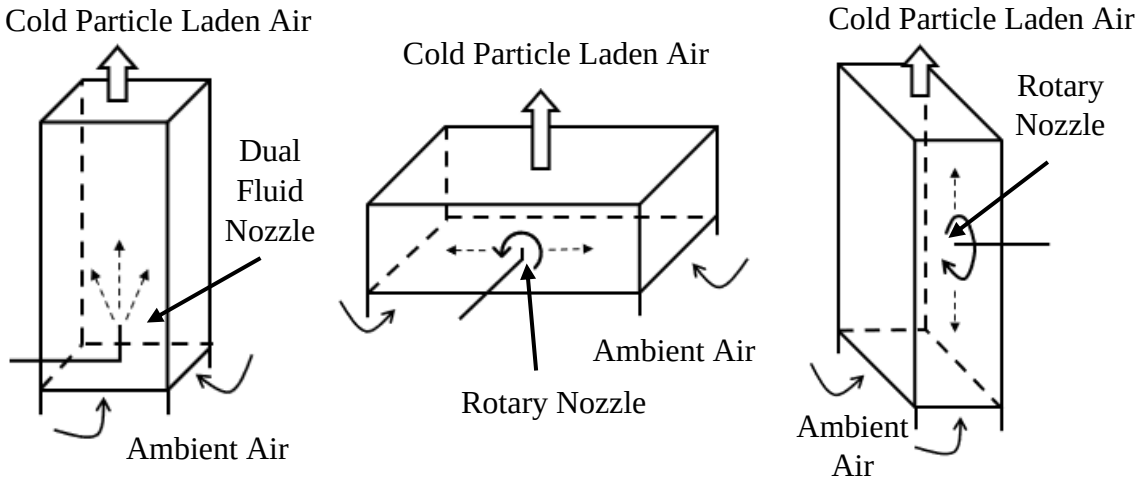


Figure 4: BETE XA-PR 050 Dual Fluid Nozzle with internal mixing.

3.1.2 Proposed Final Chamber Design

Assuming the BETE XA-PR 050 Dual Fluid Nozzle is used in the final design, the system needs to be tall but slender to take advantage of the spray angle and range of the nozzle. The chamber walls can reach almost down to the ground, leaving a small gap to allow air entering. For easy maintenance, e.g. replacement of the nozzle, one of the walls of the chamber should open. The cold air stream then leaves the evaporation chamber and is moved to the separation mechanism. Sensors monitor the ambient air as well as water and air flowrate to allow quick adaptation to changing environmental conditions. This will ensure full evaporation and maximum particle collection. If a rotary atomizer is used, the chamber must be wider to accommodate the spray angle. However, at the same time the

necessary height of the chamber would decrease. Orienting the atomizer vertically would allow empty air space to be used rather than potential farmland, see **Figure 5**.



I) XA-PR 050 Nozzle II) Rotary Horizontal Alignment III) Rotary Vertical Alignment

Figure 5: Evaporation Chamber Design Based on Nozzle choice and alignment. I) Running a XA-PR 050 nozzle requires a slender and tall frame. II) Horizontal aligned rotary atomizer requires a wide footprint but less height. III) Vertically aligned rotary atomizer require a high and deep chamber with minimal width.

3.2 The Separation System

Knowing the expected droplet size and the concentration in the drainage water, allows the calculation of the solid particle size. As the efficiency of most separation systems depends on the particle diameter, this is crucial to take it into consideration when choosing a system to prevent costly post-treatment steps.

As stated in Chapter 2.7, separation systems are subdivided into active and passive. The following section shows the benefit and limitation of each method including a quantitative analysis to determine usability. The particle size of interest in the proposed system can be calculated using the given amount of total dissolved solids from **Table 1**. Approximately 6,900 mg of minerals and elements are suspended in 1 L of liquid. It is possible to simplify the calculation by using the density of the two most common solutes, $\rho_{Sulfate}$ at $2664\,\frac{\mathrm{kg}}{\mathrm{m}^3}$ and ρ_{NaCl} at $2170\,\frac{\mathrm{kg}}{\mathrm{m}^3}$ as those two compounds accounts for 90.5 % of the total dissolved solids. Knowing that the droplet diameter ranges between 25 to 30 µm, and water has a density of $\rho_{Water} = 1000\,\frac{\mathrm{kg}}{\mathrm{m}^3}$, leads to the following set of equations for a droplet diameter of 30 µm:

$$V_W = \pi \frac{4}{3} r^3 = 1.414 \times 10^{-14}\ \mathrm{m}^3 \tag{1}$$

$$M_W = V_W \, \rho_W = 1.414 \times 10^{-11} \text{ kg} \quad (2)$$

$$C_P = \frac{M_{P,T}}{1\ L} = \frac{6{,}900\ mg}{1\ kg} = 0.69\ \% \quad (3)$$

$$M_P = C_P \, M_W = 9.755 \times 10^{-14} \text{ kg} \quad (4)$$

$$V_P = \frac{M_P}{\frac{\rho_{Sulfate} + \rho_{NaCl}}{2}} = 4.04 \times 10^{-17} \text{ m}^3 \quad (5)$$

Assuming spherical shape for simplicity reasons, the approximate precipitate particle radius is 2.1 μm (diameter 4.2 μm).

3.2.1 Active vs Passive Separation Systems

Passive Separation

Passive refers to a mechanism or equipment which does not require additional energy input for operation. As the aim is to create an affordable separation and cooling system, operating cost must be kept low. Thus, taking advantage of natural phenomena such as gravity and the inertia of solid particles is crucial. The three separation systems discussed are vertical flow systems, settling chambers and a Louvre-Type collector. However, to fully understand the assessment, the following terminology is necessary, as adapted from A. Ogawa [35] and visualized in **Table 2**:

Table 2: Particle classification based on size

Coarse Particle	X_p = 100 to 1,000 μm
Fine Particle	X_p = 10 to 100 μm
Finest Particle	X_p = 0.1 to 10 μm

The cut-size of a solid particle X_c refers to the minimum diameter that cannot be separated by the system. The particles collected by the proposed system belong into the Finest Particle Category as their diameter will range between 4 to 10 μm depending on the particle concentration suspended in the liquid.

Separation of Solid Particle in a Vertical Flow System

In the case of a vertical flow system, the cut-size is determined by setting drag force DF and gravity force G equal. Particles larger than X_c accumulate in a collection chamber at the bottom while smaller particles follow the gas flow as drag force will dominate over gravity.

Figure 6 illustrates the process.

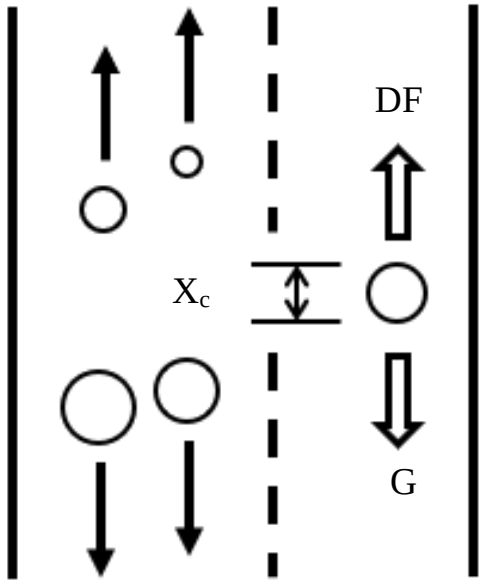


Figure 6: Particles of cut-size are at mechanical equilibrium (drag force DF = gravity force G). Coarse particles move downward while fine particles follow air stream upward.

For a stationary particle, u_p = 0, the cut-size can be obtained using equation 1 as simplified by A. Ogawa [35].

$$X_c = \left(\frac{39}{4} \cdot \frac{k \cdot \rho_P \cdot \nu_g^{\frac{1}{2}}}{\rho_g \cdot G} \right)^{\frac{2}{3}} \cdot u_g \tag{6}$$

Here, k refers to the shape of the particle: k = 1 represents a spherical particle while a shape factor of 1.76 refers to a slender-shaped particle. The density ρ is given in kg/m^3 for both the fluid (g) and particle (p). The kinematic viscosity of gas ν_g is given in m^2/s, and u_o refers to the fluid velocity in m/s. Gravitational acceleration g is set to 9.81 m/s^2. The following **Table 3** gives the cut-size for sodium chloride NaCl for various chamber footprints and an air flow rate of 0.07 m^3/s which is equivalent to 2.2 m/s in an 8“ duct . It can be seen that separation through vertical flow systems is applicable for coarse particles and when sufficient space is available to significantly reduce the air flow. Considering the estimated particle size of 4 µm at the beginning of this chapter, the flow velocity would have to be minuscule, making the chamber footprint too big in comparison to a greenhouse. As an alternative, agglomeration might be used to increase particle size rather than changing the air flow.

Table 3: Cut-Size of particles in m based on final system with $\rho_g = 1.142\ kg/m^3$ at 36 °C, $\rho_p = 2170\ kg/m^3$ and $\nu_g = 1.654 \cdot 10^{-5}\ m^2/s$.

A in [m^2]	u_g in [m/s]	Cut-size X_c in m
5	0.014	0.05
1.4	0.05	0.2
0.9	0.075	0.29
0.7	0.1	0.39

Separation using Settling Chambers

Contrary to the previous system, a settling chamber takes advantage of horizontal air flow, see **Figure 7** for reference. It is primarily applied to separate coarse particles, [35]. Coarse particles settle in the first chamber while finer particles are carried further in the air stream. It is often used as a pre-filtering device when dealing with high dust concentration.

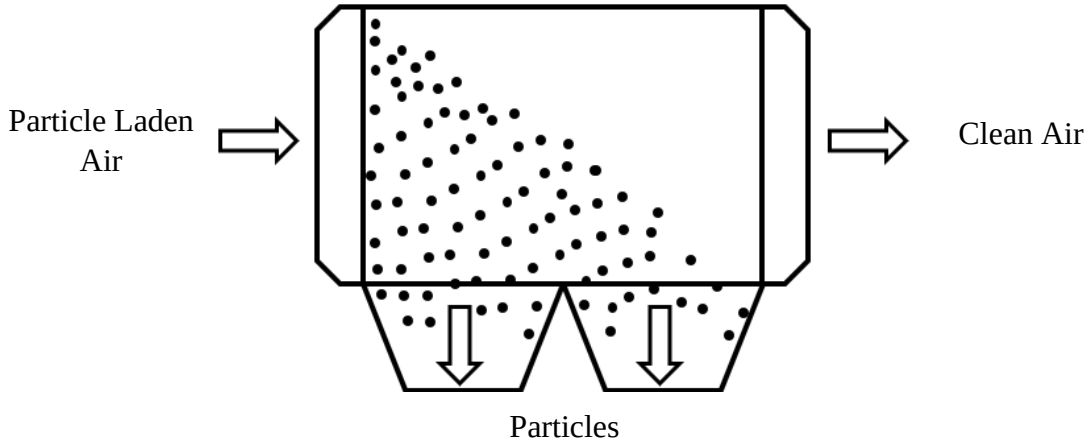


Figure 7: Simple settling chamber. Air laden with particles enters the chamber from the left. Gravity forces the particles to fall into dust bins along the way. Clean air exits the chamber.

The efficiency of settling chambers depends on the chamber residence and particle settling time which are influenced by the air flow velocity and terminal velocity of the particle. According to the Environmental Protection Agency (EPA) [36], the collection efficiency η can be written as:

$$\eta = 1 - e^{-x} \tag{7}$$

Here, x is the ratio of chamber residence time t_r to particle settling time t_s for a simple settling chamber. The residence time can be calculated using the following expression, where the chamber length is given in m and the gas velocity is given in m/s. However, the velocity can be replaced by the air mass flow rate *Q* per chamber area in m^2 (height *H* times width *W*):

$$t_r = \frac{L}{u_g} = \frac{L}{\dot{m}_a} \cdot A = \frac{L}{\dot{m}_a} \cdot HW \tag{8}$$

The particle settling time is given as followed:

$$t_s = \frac{H}{u_t} \tag{9}$$

u_t is the terminal velocity of the particle in m/s. The terminal velocity for low Reynolds numbers Re < 4 is:

$$u_t = \frac{G\rho_p d_p^2}{18\mu_g} \tag{10}$$

Where g is the acceleration of the particle due to gravity set to 9.81 m/s^2, ρ_p is the particle density for NaCl in kg/m^3, μ_g is the gas viscosity in kg/ms and d_p is the particle diameter in m. Replacing x with equation (3) to (5) yields the following expression:

$$\eta = 1 - e^{-\left(\frac{G\rho_p LW}{18\mu_g \dot{m}_a}\right) d_p^2} \tag{11}$$

The following **Table 4** and **Figure 8** show the size requirements for a simple settling chamber with flowrate 0.07 m^3/s which is equivalent to an air velocity of 2.2 m/s in an 8“ supply duct. The efficiency of interest ranges from 50%, 75% to 90% with particle size varying from 5 µm to 10 µm at a viscosity of $1.895 \cdot 10^{-5}\,\frac{kg}{ms}$. **Equation 11** was modified to obtain the required footprint:

$$LW = -\frac{\ln(1-\eta)\, 18\mu_g \dot{m}_a}{G\rho_p d_p^2} \tag{12}$$

The smaller the particles, the bigger the required footprint of such a system. **Table** 4 confirms the statement made by A. Ogawa [35] that settling chambers should primarily be used for coarse particles. Satisfactory efficiencies for particles below 10 µm would require a separation chamber multiple times the size of the greenhouse. However, it is possible to increase the settling rate substantially through agglomeration. Settling time t_s depends on the terminal velocity v_t which is proportional to the square of the particle size, see **Equation 9** and **10**. Doubling the particle diameter results, decreases t_s to a quarter of its original duration. A possible method of agglomeration is the use of ultrasonic waves, see K. Sutherland [37]. Nevertheless, those additional treatments would increase the operation cost of the proposed system, thus making it less competitive to common cooling methods in greenhouses.

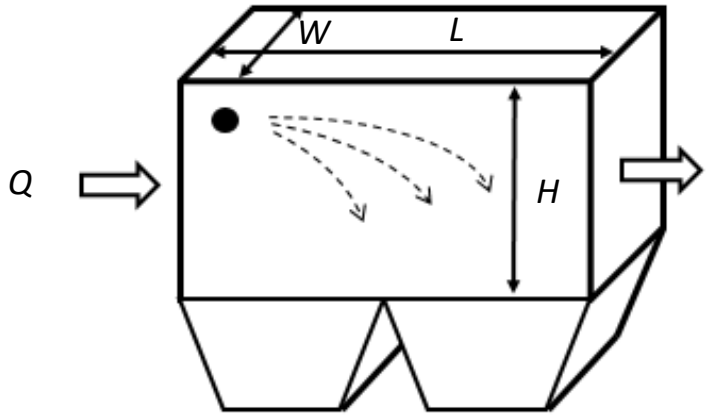


Figure 8: Settling chamber dimensions for a simple settling chamber.

Table 4: Footprint of simple settling chamber for particle size 5 μm, 7.5 μm and 10 μm and efficiency of 50%, 75% and 90% at an air flow rate of 0.07 m^3/s

Air Flow m^3/s	Particle Size μm	Efficiency %	Footprint m^2
0.07	5	50	31.1
		75	62.2
		90	103.3
	7.5	50	13.8
		75	27.6
		90	45.9
	10	50	7.8
		75	15.5
		90	25.8

Louver-Type Separators

Contrary to previous systems which took advantage of gravity, the Louver-Type Separator is classified as an inertial separator, [35]. Using the inertia of the particle and air velocity between 5 to 10 m/s, collection efficiency is high for particles between 4 to 100 μm, J. B. Sim et al. [38]. Collection efficiency can be improved by changing the design of the dust container as well as Louver Blade. **Figure 9** shows the basic principles of a Louvre-Type Separator.

Air flow laden with dust enters the chamber and hits the blades. The majority of the air passes through the blades and leaves the chamber as clean air. A smaller flow, called blowdown carries the solid particles out of the separation chamber without passing through the blades due to their high inertia.

Figure 10 shows the modified system as used by J. B. Sim et al. [38] which simplifies the process. Instead of a blowdown, the particles are captured in a dust container which would reduce the amount of cold air lost to the GH. Different dust container shapes can further increase efficiency by improving particle trajectory, cut-size and pressure drop.

In addition, blade design modifications, i.e. angle, length and shape aid particle separation as well, see [35],[38], [39] and [40]. G. Musgrove et al. [40] for instance determined that particles with diameters below 7 μm are easier to collect using less but longer louver blades.

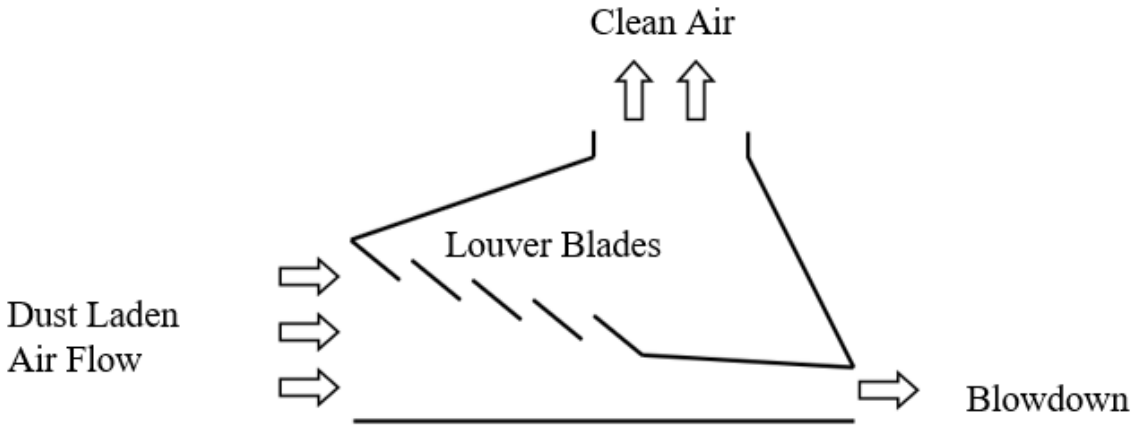


Figure 9: Basic Louver-Type Separator adapted from J. L. Smith and M. J. Goglia [39]

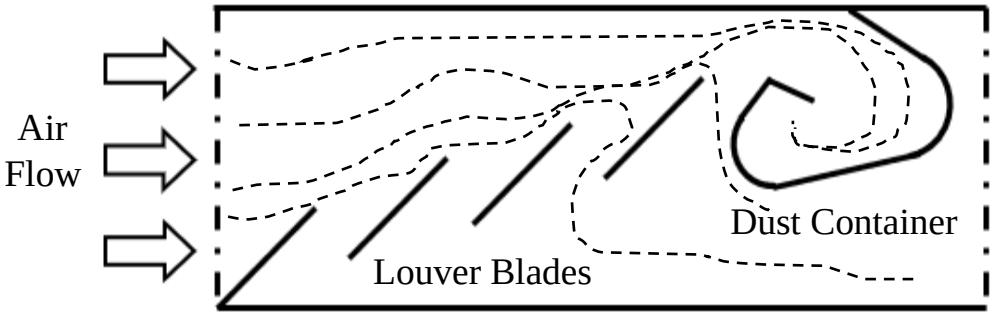


Figure 10: Modified louver separator schematic with dust container and simplified particle trajectory, adapted from J.-B. Sim et al [38]

Due to size limitation and the estimated particle diameter of 4 μm, the louver blade seems the most sensible choice for passive separation method as no complicated pre-treatment steps to agglomerate the particles are required and it is easy to build and operate. In addition, the footprint of the separation system would be negligible in comparison to the greenhouse and evaporation chamber.

Active Separation

All separation methods which require the direct use of additional energy are referred to as active separation systems. Using electricity to run the system is undesirable due to the extra cost added to the operation. However, depending on the particle size, type and particle count in the flow, those systems can be the only ones able to filter the air. A. Ogawa [35] gives a detailed overview of the different active separation systems in use, their power usage, space requirements and cut-size, which helped narrow down the possible systems to three: bag filter, cyclone separator (CS) and electrostatic precipitator (ESP).

Electrostatic Precipitator

ESPs were first implemented at the turn of the last century to reduce acid mist and particulate matter. Since then, they have been continuously researched to increase their efficiency and reduce operating cost. Their major advantage is the lack of pressure drop as gas can flow freely between the collection plates. According to EPA [41], the collection process can be divided into three steps which are illustrated in **Figure 11**:

1) Charging of the particle and movement towards collection plates
2) Settling of particles after dislodging them from the collection plates
3) Removal of particles from hopper

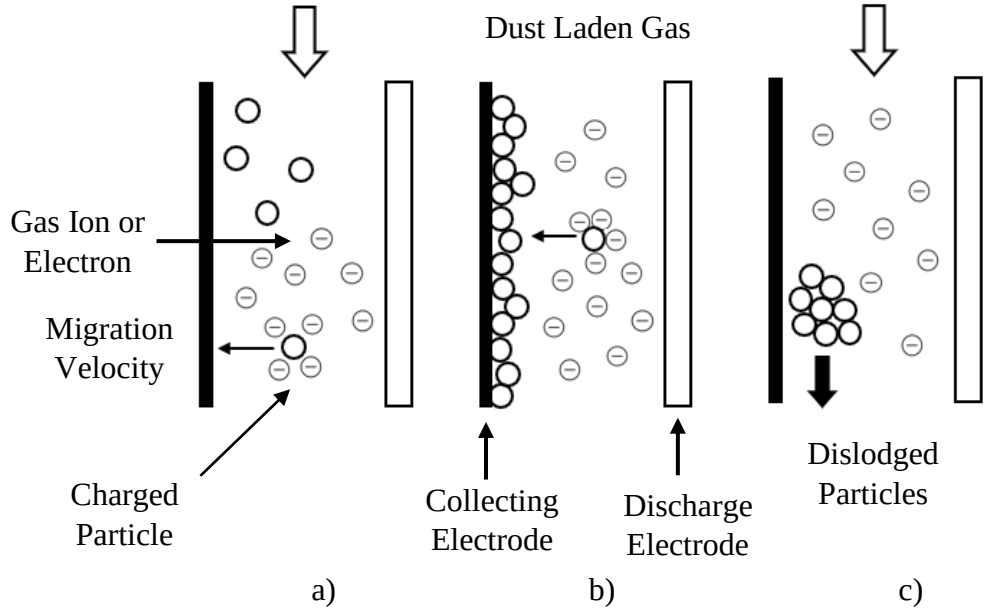


Figure 11: Particle separation using electrostatic precipitator. a) Corona voltage at discharge electrode produces ions and electrons. Ions attach to the Particles. b) Particles accumulate on collecting electrode due to coulomb force. c) Particle layer builds up over

time. Mechanical tapping of the collecting electrode dislodges material. Particles are collected in hopper below. See A. Ogawa [35] and A. Mizuno [42].

Following EPA guidelines [41], ESPs are most effective if the dust particles have a moderate electric resistivity, $5 \cdot 10^8$ to $5 \cdot 10^{10} \Omega$ cm and particle size is below 0.2 µm or above 1.0 µm [43]. Sodium Chloride (NaCl) has an electric Resistive of $10^8 - 10^9$, see Y. Zhuang et al. [44], and upon evaporation, the particles will have a diameter of at least 4 µm and are therefore suited for collection via ESPs. In addition, the pressure drop associated with ESPs is less than 100 Pa, far less than for any other active separation system. See **Table 5** for comparison.

Bag Filters

Even though a filter itself does not require electricity to run, the pressure drop associated with the setup is approximately 1000-1,500 Pa, which requires the use of powerful fans, see R. Zevenhoven and P. Kilipen [45]. Thus, the energy usage of bag filter separation systems is of the same order as other active filtration systems such as CS and centrifugal separators at 110 kW per 100,000 m^3/h gas flow rate, [35]. Contrary to ESP, the filter's efficiency does not depend on the electric resistivity of the medium, and the filtering size range is expandable depending on the type of filter used, i.e. textile, plastic or ceramic. However, according to R. Zevenhoven and P. Kilipen [45], bag filters are prone to filter blinding which occurs when small particles accumulate in the filter, rapidly increasing the pressure drop. They recommend applications with a wider particle size distribution to slow down build up on the filter surface. **Figure 12** illustrates the basic concept of a bag filter system. Dust laden gas passes through the filter from the inside and leaves particle-free at the top of the chamber. Once a maximum pressure drop is reached, the filters have to be cleaned. During cleaning, the dusty air stream is stopped – either for all bags, or in the case of pulse-jet cleaning, for one bag filter at a time. The caked-on particles fall down and are collected at the bottom of the system. See [45] for a more detailed description.

Cyclone Separator

Similar to Louver-Type Separators, CS are part of the inertial separation systems. However, due to the substantially higher pressure drop, they can be classified as an active system. **Figure 13** illustrates the operation principles. Air is introduced to the system off centre which induces a vortex. As a result, coarse particles are ejected from the main fluid stream due to their high inertia while smaller particles are able to follow the stream. The particles accumulate in the dust bunker at the bottom. The cut-size decreases with higher stream velocity. For more information, refer to A. Ogawa [35] and K. Sutherland [37].

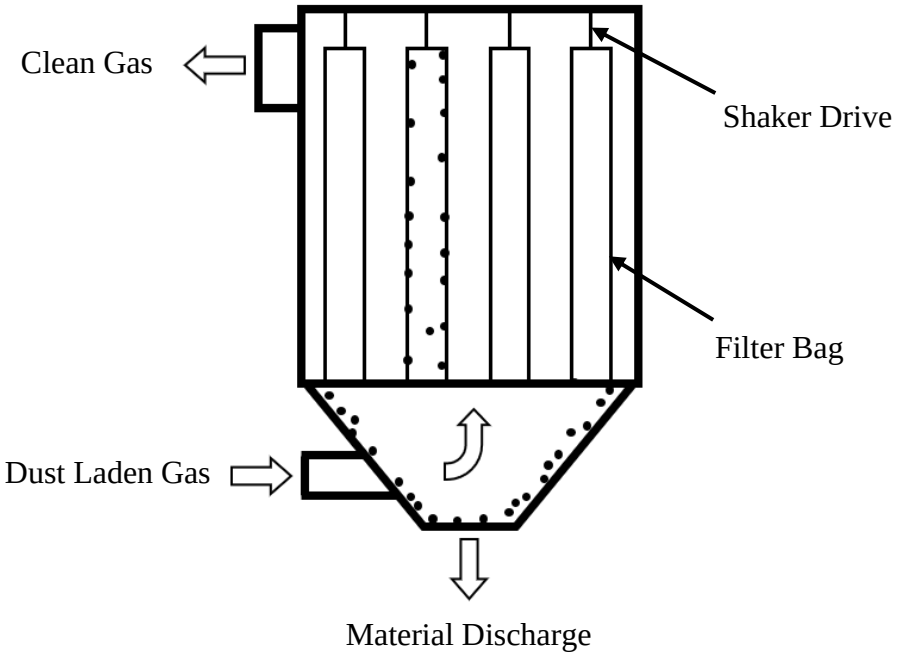


Figure 12: Basic bag filter separation system

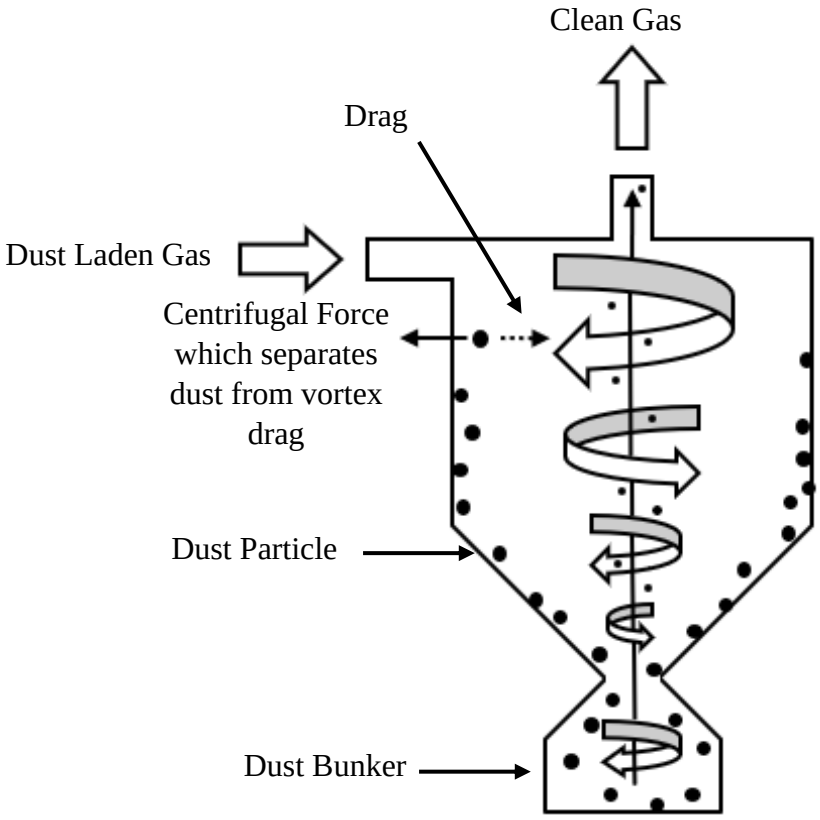


Figure 13: Centrifugal separator and operating principles

Quantitative Separation Comparison

Table 5 reproduces data provided by A. Ogawa [35] for power usage, pressure drop and cut size, along with data for the Louver Separator from [38]. The separation systems are listed from smallest pressure drop to biggest which coincides with the energy dissipation. The energy dissipation is based on the (ideal) power consumption of the fan required to move the fluid, see [46].

Table 5: Separation Systems Sorted by Cut Size Xc, Gas Velocity, Pressure Drop, Energy Dissipation, Operating Temperature and Required Operating Space adapted from A. Ogawa [35] and expended with data from [38].

System	Cut Size	Gas Velocity	Pressure Drop	Energy Dissipation	Operating Temperature	Required Space
	X_c in μm	u_0 in m/s	ΔP in Pa	kW/1000 m^3hK	T in K	m^3/1000 m^3
Settling Chamber	35	0.5 – 2.0	10-40	0.01-0.04	773	8-12
Electrostatic Precipitator	0.5-1	0.5-1	30-100	0.1-0.3	473-573	8-12
Louvres-Type	3.5-8.5	3-10	300-400	0.09-0.1	Limited by Melting Point of Material	
Cyclone Separator	10-60	12-18	400-1200	0.25-0.75	673	0.5-5
Bag Filter	0.5-1	-	500-1500	0.3-1.1	373	2.7-5

Considering that the size of an ESP can be reduced through strategic placement and shape of the collection and discharge electrodes, it appears to be the most appropriate choice for an active separation system. The energy input necessary for a cyclone separator or bag filter would make the system too costly to be competitive with alternative cooling systems. The footprint required for an ESP would be negligible in comparison to the evaporation chamber and greenhouse, similar to the Louvres-Type separation system.

3.2.2 Proposed Final Separation Design

The separation system is directly attached to the outlet of the evaporation chamber. Cold air laden with particles enters the separation mechanism while clean air is released into the greenhouse. Each system is mounted individually in-line with the airflow but can be mounted in series to increase collection efficiency if necessary.

Figure 14a shows a schematic of the separation process while

Figure 14**b** shows a real experimental system with the Louver-Type Separator mounted.

A prototype louver-type separator has been constructed for use in experiments. It has a total length of 300 mm, width and height of 100 mm and is made from clear 1/8" acrylic. The four 2" wide blades are angled at 40° and spaced 1" apart. At either end of the separator, flanges are mounted that allow airtight connection to the air duct, see **Figure 15.**

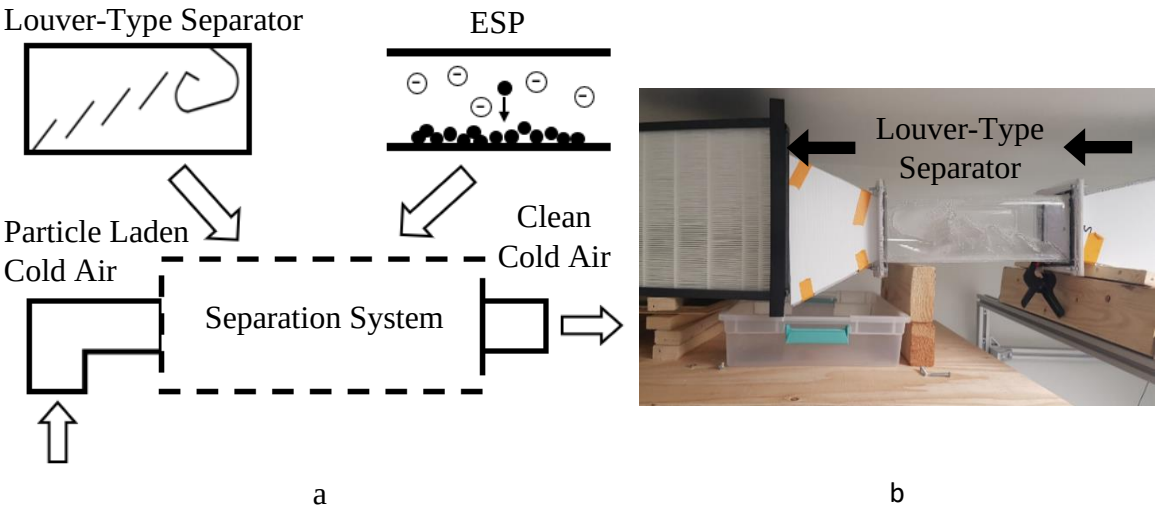


Figure 14: a) Schematic of separation system with the two separation mechanisms chosen, louver-type and electrostatic precipitator. Cold particle laden air enters the system and clean cold air is released into the greenhouse. b) Separation system in experimental setup including HEPA filter to prevent aerosols in the lab.

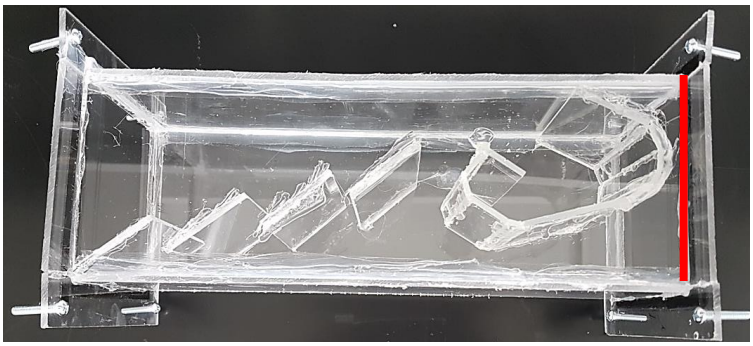


Figure 15: Louver Type Separator. Length is 300 mm, widht is 100 mm and height is 100 m. Red line is 100 mm long.

3.2.3 Salt Collection

Ideally, only solid particles will be collected in the separation system. In a Louver-Type separator, most of the particles would accumulate in the dust chamber with minor portions attached to the Louver-blades. The blades and chamber could be removed individually. Particles accumulated on them would be shaken into a storage container and stored until disposal. The parts of the separator would then be reinserted, and the system

could run again. To time the maintenance intervals, small weight sensors could be attached to keep track of the particle accumulation.

In principle, the ESP runs just like the Louver Separator. Major difference, after removing the collecting electrode for tapping, a quick rinse is recommended. Again, the particles are shaken into a container until the times for disposal.

The exact amount of particles collectable depends on the NaCl concentration. Higher salt content will increase salt removal rate but also pose a higher risk of clogging the system. The particles shaken off after each experiment in conjunction with the initial salt content, allow for the calculation of the collection efficiency. Ideally, the efficiency should be above 90 % to ensure plants are not covered by minerals and salt.

3.3 Proposed Final System Design

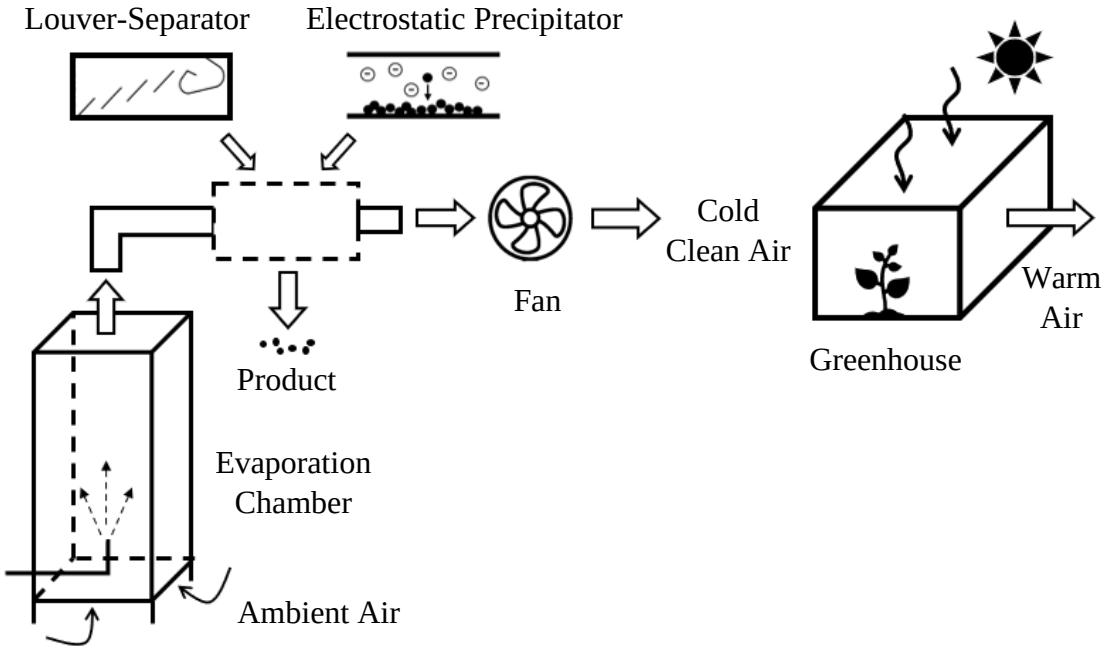


Figure 16: Final system design including all components. Ambient air is sucked into the ECH by the fan. DI water and later 1% NaCl solution is atomized by the nozzle. Colder and more humid air laden with salt particles, leaves the chamber. A separation system – either louver-type or ESP then separates the solids from the air stream. Cold, clean air enters the GH and moved to the exit. As the sun is heating the GH, a warmer and less air flow leaves the system.

4. System Modeling

To determine performance of the evaporation chamber for a range of operating conditions and the approximate size of the evaporation chamber in relation to a greenhouse, a simplified thermodynamic and heat and mass transfer model is needed. Relevant ambient conditions are inlet temperature and humidity. Operating parameters are air and water flow rates. As the size of the evaporation chamber heavily depends on the time needed to evaporate a water droplet, the model must account for different droplet diameters. Solar radiation is the primary heat input into the greenhouse. The model will pinpoint the exact operating conditions required to run a reasonably sized system to produce ideal plant environment. The model can be separated into two systems, the evaporation chamber (System I) and the greenhouse (System II), as shown in **Figure 17**.

4.1 Thermodynamic Model

The thermodynamic model assumes steady state operation. Ambient hot air at temperature T_1 is forced into the chamber at rate $\dot{m}_a$, while water at temperature T_W, atomized by air, is supplied to the chamber at a rate of $\dot{m}_w$ (and $\dot{m}_{ap}$ for the atomizing air). Heat loss (in the laboratory, heat gain in application) through the chamber walls is accounted for by $\dot{Q}_{Loss}$. Colder and more humid air leaves the drying chamber at T_2 before entering the green house. The sun then heats the air at a rate of $\dot{Q}_{Sun}$ resulting in a temperature of T_3 and a lower relative humidity at the greenhouse exit. $\dot{Q}_{Sun}$is normalized per 1 m^2 of greenhouse. The red dotted line in

Figure 17 shows the separation between the evaporation chamber and greenhouse systems and their shared boundary, at location ②. The terms $\dot{m}_{v1}, \dot{m}_{v2}$ and $\dot{m}_{v3}$ account for the water content in the air. All extensive quantities are normalized by the greenhouse area.

To increase the evaporation rate, the water is atomized by a spray nozzle to increase surface area and minimize overall droplet size. As an upper boundary of operation, the preferred vapor pressure deficit (VPD) for commercially grown tomatoes is used as the target average condition for the greenhouse. Preferred VPD ranges between 0.5 to 1.2 kPa [47]. The VPD describes the difference between the partial pressure of water in the air and the saturation pressure of water at the air temperature and depends directly on the air temperature and relative humidity (see **Equation 13** to **15**). The saturation vapor pressure P_g was calculated using the Buck equation while the air vapor pressure was calculated using P_g and relative humidity (RH).

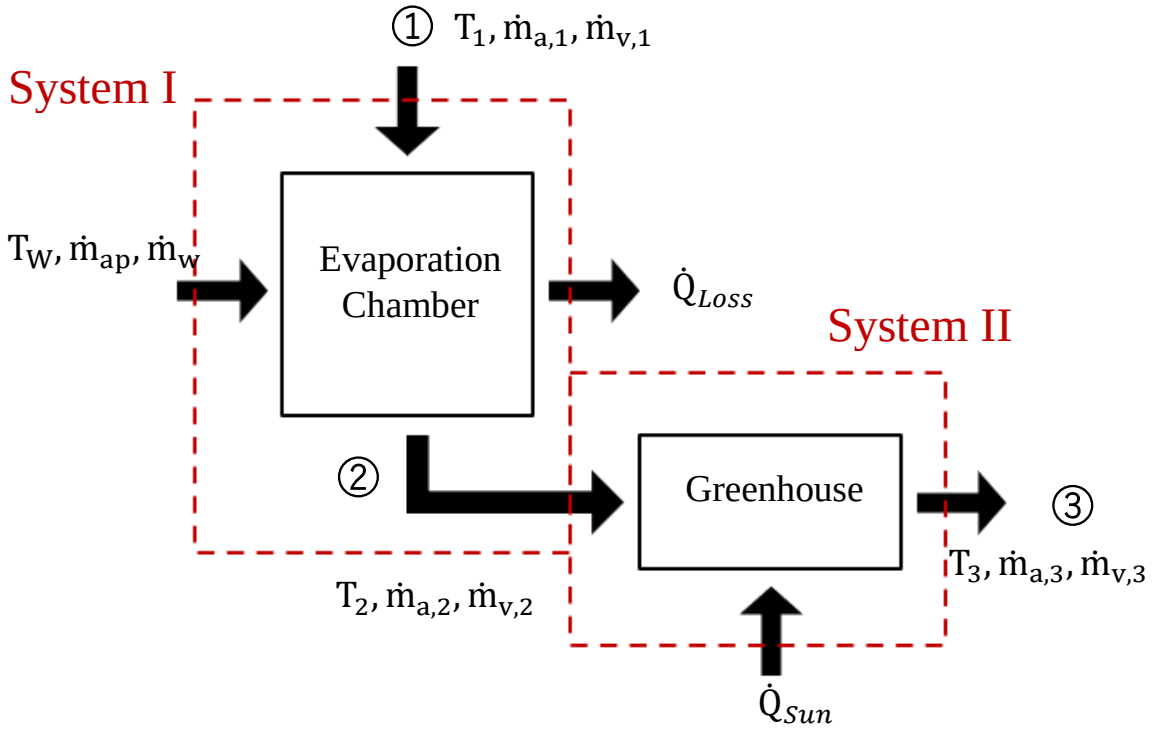


Figure 17: Schematic of heat transfer model including relevant variables.

$$VPD = P_g - P_v \tag{13}$$

$$P_g = 0.61121e^{\left(18.678-\frac{T}{234.5}\right)\left(\frac{T}{257.14+T}\right)}, P_g \text{ in kPa} \tag{14}$$

$$P_v = RH \cdot P_g \tag{15}$$

System I

The first system yields the following governing equation in terms of energy conservation, where $\dot{m}_{a1}$ describes the air added to the system through the fan and $\dot{m}_{ap}$ the air added by the dual fluid nozzle.

$$\dot{Q}_{Loss} = \left(\dot{m}_{a1}h_{a1} + \dot{m}_{ap}h_{aw} + \dot{m}_{v1}h_{v1}\right) + \dot{m}_w h_w - \left(\dot{m}_{a2}h_{a2} + \dot{m}_{v2}h_{v2}\right) \tag{16}$$

The relationship between $\dot{m}_{a1}, \dot{m}_{a2}$ and $\dot{m}_{a3}$ is as follows:

$$\dot{m}_{a2} = \dot{m}_{a3} = \dot{m}_{a1} + \dot{m}_{ap} \tag{17}$$

The amount of heat lost by the chamber is equal to:

$$\dot{Q}_{Loss} = \left(\dot{m}_a + \dot{m}_{ap}\right) c_{pa} \Delta T \tag{18}$$

Where ΔT refers to the temperature difference between the inlet and outlet of the chamber when the system is operated without water at steady state. This is a negative quantity in application but positive in the laboratory as ambient air is colder than the chamber temperature. Dividing the mass flow rate of the water vapor by the air mass flow, yields the humidity ratio:

$$w_1 = \frac{\dot{m}_{v1}}{\dot{m}_{a1}}$$
$$w_2 = \frac{\dot{m}_{v2}}{\dot{m}_{a2}} = \frac{\dot{m}_{v1} + \dot{m}_w}{\dot{m}_{a1} + \dot{m}_{ap}} \tag{19}$$

Which can also be expressed in terms of partial pressure and ambient pressure:

$$w = 0.622 \frac{P_v}{P_{atm} - P_v} \tag{20}$$

System II

After determining the temperature and relative humidity at ②, the corresponding VPD can be calculated using Equations 13 to 15. The second governing **Equation 21** is then used to calculate the relative humidity and temperature at the outlet of the greenhouse, position 3:

$$0 = (\dot{m}_{a2} h_{a2} + \dot{m}_{v2} h_{v2}) - (\dot{m}_{a3} h_{a3} + \dot{m}_{v3} h_{v3}) + \dot{Q}_{Sun} \tag{21}$$

This allows for the calculation of the VPD at ③**.** The average of the temperatures and relative humidity at ② and ③ enables the calculation of a mean VPD value in the greenhouse VPD_{GH} as well as T_{GH} and RH_{GH}. Knowing the operation range of VPD for commercial tomato plants of between 0.8 and 1.2 kPa, makes it possible to determine the correct water and air flowrates needed at a certain inlet temperature and RH and insolation to achieve a specific VPD. Additionally, knowing the air flowrate, relative humidity and temperatures at ① and ②, allows the calculation of the expected evaporation time (EET) for small droplets in the evaporation chamber. As a result, one can predict the chamber size needed to evaporate a specific water flow and obtain an acceptable grow climate for the plants.

4.2 Droplet Evaporation Time

According to [48], the time required by a small water droplet $d_d \leq 230$ µm to fully evaporate can be calculated as follows:

$$ETT = \frac{d_d^2}{q_0 \Delta T} \tag{22}$$

Evaporation time for a pure water droplet should represent an upper bound for evaporation time. NaCl in solution reduces the overall water amount per droplet volume, thus reducing the time needed for complete evaporation. Literature studies [49] show a significant reduction in evaporation time for NaCl-water droplets versus pure water droplets. q_0, given in **Equation 23**, depends on the parameters a and b which relate to the ambient conditions and liquid properties along with the constant $s_0 = -1.117 \cdot ms^{-0.5}$. ΔT is the difference between ambient temperature T_{amb} and wet-bulb temperature T_{wetb}. However, contrary to the model in [48], T_{amb} here is taken as the mean of the inlet temperature, T_1, and outlet temperature, T_2, of the evaporation chamber. Choosing T_1 for the ambient temperature would underestimate the evaporation time as the system is providing a continuous spray which experience a varying environment during evaporation. A small number of droplets would barely change the ambient temperature of a large air stream while a substantial and continuous spray will drop the chambers' ambient temperature to some value between T_1 and T_2.

$$q_0 = \frac{2a}{\Delta T}(1 + bs_0) \tag{23}$$

Parameters a and b are calculated as given in **Equation 24** to **25**. Here, M_L is the molecular weight of the evaporating liquid, ρ_L gives the density of the liquid, γ can be approximated as a constant of ~ 67 Pa/K, T_f is the temperature of the droplet film, assumed to be T_W while R is the gas constant of $R = 8.3144\, J/mol^{-1}K^{-1}$. For **Equation 24** both the density of air ρ_a and viscosity η_a are determined at T_f.

$$a = \frac{4\,\gamma\, M_L D_{v,f}}{\rho_L R}\left(\frac{\Delta T}{T_f}\right) \tag{24}$$

$$b = 0.276\left(\frac{\rho_{a,f}}{\eta_{a,f} D_{v,f}^2}\right)^{\frac{1}{6}} \tag{25}$$

The diffusion coefficient of water vapor in air at T_f, $D_{v,f}$, is approximated using:

$$D_{v,f} = 21.2 \cdot 10^{-6}(1 + 0.0071\, T_f) \tag{26}$$

After calculating the evaporation time, it is possible to define the required footprint for the chamber per 1 m^2 of greenhouse for a specific VPD and air flow rate $\dot{m}_a$, based on a given maximum height for the evaporation chamber, H_{ECH}.

$$A = \frac{\dot{m}_a}{\rho_a}\left(\frac{ETT}{H_{max}}\right) \tag{27}$$

The target VPD is achievable with a multitude of air flow and water flow combinations. Evaporation time is determined by the droplet size, inlet conditions (temperature and humidity) and air flow rate. To ensure full evaporation, the velocity of the air stream needs to provide sufficient residence time for the droplet in the chamber. Thus, for a given airflow, there is a specific chamber area which makes the target VDP possible per 1 m^2 greenhouse area.

Thus, the thermodynamic and kinetic models allow accurate description of the overall system dimension, and water usage and will allow the calculation of estimated energy consumption based on the air flow rate.

4.3 Modeling results

The following section shows the expected behavior of System I and the full system including droplet evaporation based on the input variables: $T_{in}, RH_{in}, \dot{m}_a, \dot{m}_w, Q_{Sun}, d_d, H_{ECH}$ and governing **Equations 16** and **21** provided above. The influence of different operating conditions on the size and performance of the system can be seen.

4.3.1 System I

The model is applied to understand the performance of the system under a variety of conditions. The trend lines in the following figures show the behavior of the evaporation process over a range of inlet conditions. In general, for fixed water flow, high air flow rates, $\dot{m}_a$, increase outlet temperature T_2 and result in low absolute humidity w_2. Conversely, higher air flow rates can evaporate more water for given outlet temperature and humidity. The functionality of the chamber is demonstrated in **Chapter 5** by comparing the predicted values of outlet temperature and humidity for the experimental conditions to the measured ones.

Changing the inlet temperature from 30 to 36 °C and maintaining a relative humidity RH_1 of 15 %, increases the predicted outlet temperature T_2 and decreases the outlet absolute humidity w_2. Compare **Figure 18a** at 22 mL/min and 0.05 $kg/s/m^2_{GH}$ where the initial outlet temperature is 10.2 °C and humidity ratio is 0.011 kg_w/kg_{da} to **Figure 18c** where T_2 is 16.2 °C and w_2 is 0.013 kg_w/kg_{da}. This shows that higher inlet temperatures allow more water evaporation at the same air flow which matches the general heat and mass transfer concept that warmer climate aids evaporation.

Changing the inlet humidity RH_1 from 15 % to 25 % while maintaining T_1 at 30 °C, increases the outlet humidity. Compare

Figure 19a-c. Thus, having an initial lower humidity allows more water evaporation at the same air flowrates.

Inlet temperature and air flow rate have strong influences on the outlet temperature of the evaporation chamber, T_2. However, greenhouses need a specific amount of cold air to remove the heat which they accumulate. Thus, changing the air flow rate to compensate for fluctuations in ambient conditions is difficult. Similarly, one is restricted to the available inlet temperature as no additional heating sources are operating in the system.

Adjusting the water flowrate makes it possible to compensate for temperature and relative humidity changes and provide a consistent cold air stream to the GH.

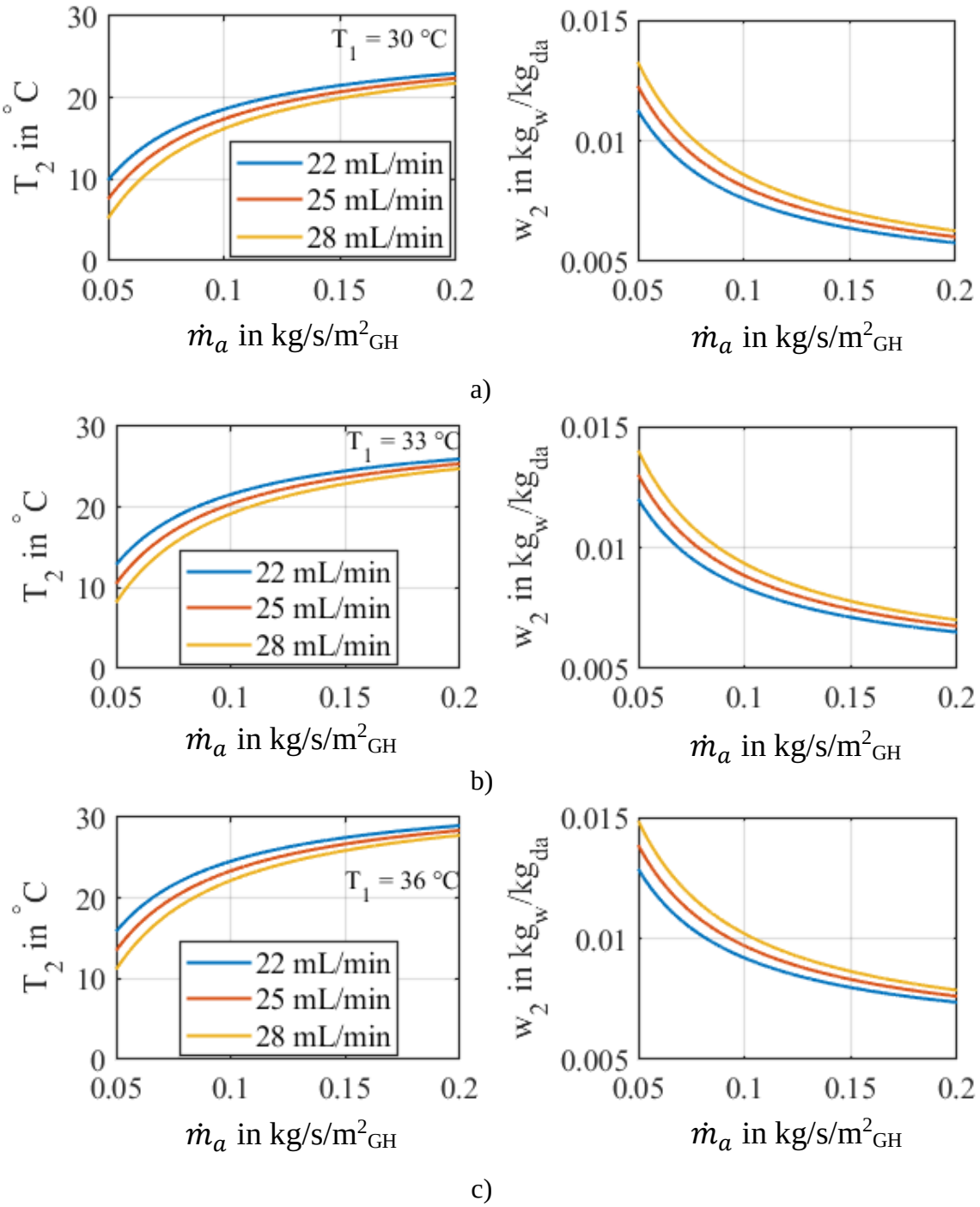


Figure 18: Outlet temperature T_2 and humidity ratio w_2 versus air flow rate $\dot{m}_a$ for different inlet temperatures, T_1 a) 30 °C, b) 33 °C and c) 36 °C all at 15 % inlet relative humidity RH_1. Water temperature is T_W = 22 °C and ΔT used to calculate Q_{Loss} is 2.24 °C. Water flow rate m_w ranges from 22 to 28 mL/min as shown in legend.

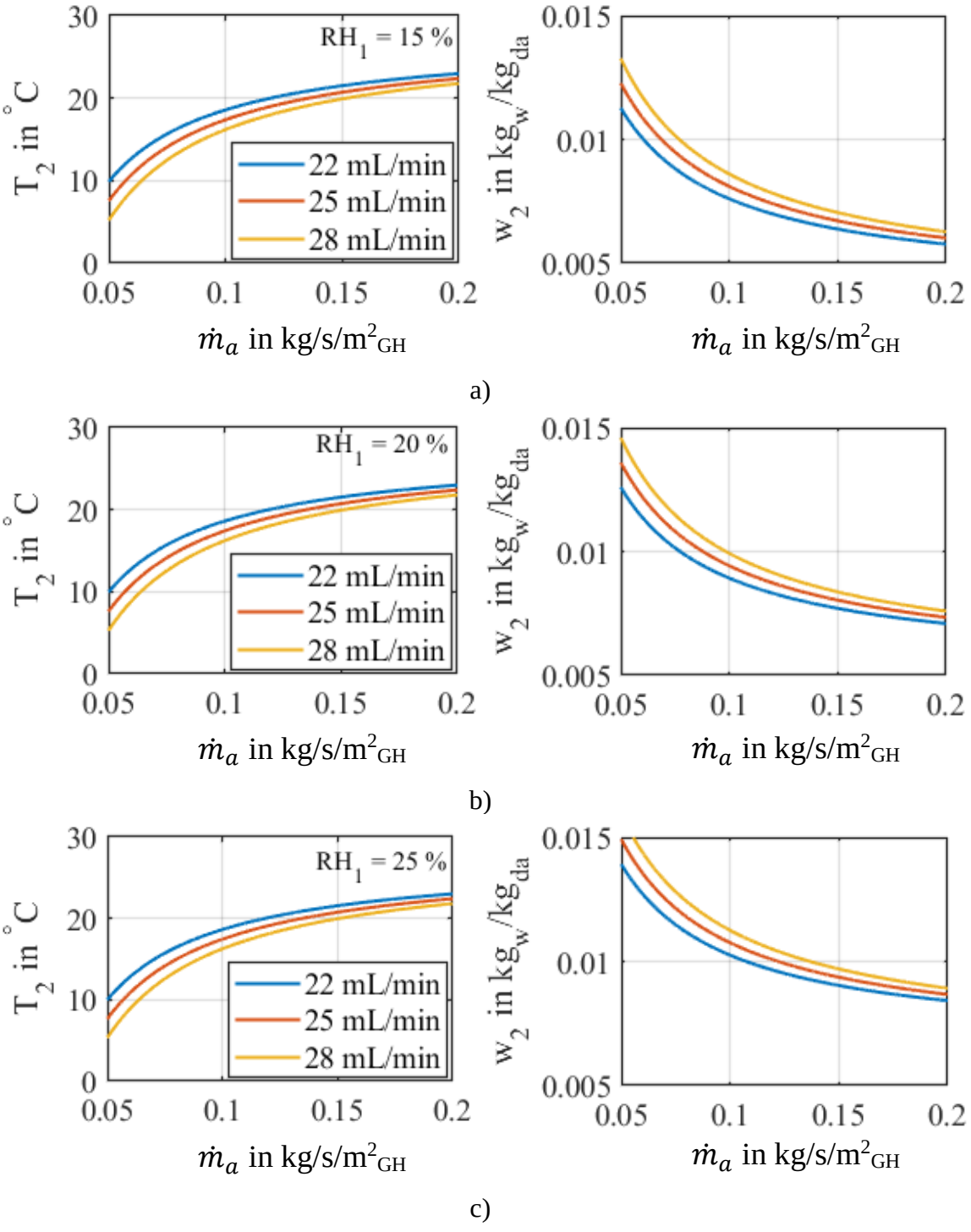


Figure 19: Outlet temperature T_2 and absolute humidity w_2 versus air flow rate for different inlet relative humidity's, RH_1 a) 15 %, b) 20 % and c) 25 % all with 30 °C inlet temperature T_1. Water temperature is T_W = 22 °C and dT used to calculate Q_{Loss} is 2.24 °C. Water flow rate $\dot{m}_w$ ranges from 22 to 28 mL/min.

4.3.2 Full System

Combining System I and System II allows the calculation of an acceptable operating range for the greenhouse for a given inlet temperature, humidity and heat rate Q_{Sun} at different air and water flowrates. **Figure 20** shows how T_{GH}, RH_{GH} and VPD_{GH} change for water flowrates $\dot{m}_w$ = 22 mL/min to 28 mL/min at T_1 = 30 °C, 15 % inlet humidity and Q_{Sun} = 0.5 kW/m^2. **Figure 22** shows how T_{GH}, RH_{GH} and VPD_{GH} change for Q_{Sun} = 0.75 kW/m^2. As VPD depends on both saturation pressure for water P_g and water vapor pressure in the air P_v, VPD is a function of relative humidity and temperature, see **Equation 13 to 15**. Low water flow increases T_2, and T_3 see **Figure 18a-c** and **Equation 21**, which leads to higher T_{GH}, which is considered as the average of T_2 and T_3. Similarly, the relative humidity decreases which reduces the water vapor partial pressure. Therefore, low water flow rates result in higher VPDs as the difference between P_g and P_v increases.

As mentioned previously, a VPD between 0.5 kPa and 1.2 kPa is deemed ideal for tomato growth. The following figures show the influence ambient conditions have on the operating conditions required for a specific VPD. **Figure 20** illustrates the influence of water flow rate on VPD_{GH}. Higher water flow rates lead to lower VPD_{GH} and smaller difference between P_g and P_v as RH_{GH} decreases. The red line in **Figure 20** marks $\dot{m}_a$ = 0.095 kg/s/m$^2_{GH}$ which will be used as a reference for further discussion. This air flow results in a VPD_{GH} = 1.0 kPa at $\dot{m}_w$ = 25 mL/min.

Figure 21 shows the influence increasing inlet temperature from T_1 = 30 °C to 33 °C has on the relative humidity and temperature inside the greenhouse at RH_1 = 15% and Q_{Sun} = 0.5 kW/m. T_{GH} increases while RH_{GH} is reduced. This means that the pressure difference between P_g and P_v is higher at reference flow rate $\dot{m}_a$ = 0.095 kg/s/m$^2_{GH}$. Hence, an increase in T_1 leads to lower air flow rates to maintain a given VPD_{GH}.

Figure 22 shows that, similar to a warmer inlet temperature, a higher Q_{Sun}, increases the overall temperature in the greenhouse across the whole air flow range. Simultaneously, the humidity RH_{GH} decreases. The air flowrate necessary to maintain a VPD_{GH} of 1.0 kPa at Q_{Sun} = 0.75 kW/m^2, T_1 = 30 °C and RH_1 = 15% decreases to 0.082 kg/s/m$^2_{GH}$, similar to **Figure 21.**

Figure 23 shows that increasing the inlet temperature T_1 to 33 °C in combination with an increase of Q_{Sun} to 0.75 kW/m^2 drastically drops the necessary airflow to maintain VPD_{GH} of 1.0 kPa. However, this will result in a significant increase in greenhouse temperature. Greenhouses rely on a steady climate for their plants. High water throughput is also a goal of the current system to maximize drainage water and salt disposal. Rather than reducing air flow, water flow rate can be increased to operate at the desired VPD_{GH} while maintaining lower greenhouse temperatures.

For optimum operation condition, low airflow rate and high-water throughput are desirable. This would keep the cost for the fan low and allow farmers to maximize the usage of their drainage water. However, exact predictions of actual operating conditions are difficult, as the sun intensity varies with location and time throughout the day. An adaptive system that automatically regulates the water input to maintain a specific air flow and VPD is the best way to compensate for those changes.

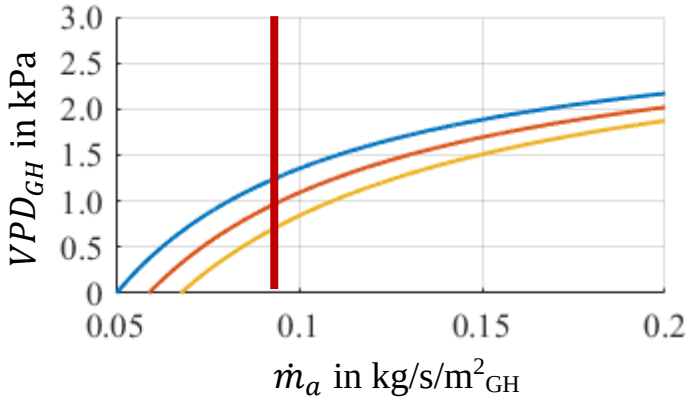
The models also serve to guide design of the cooling system.

Figure 24 and **Figure 25** show that droplet size is the major influence on EET while change in T_1 and RH_1 only have a minor influence.

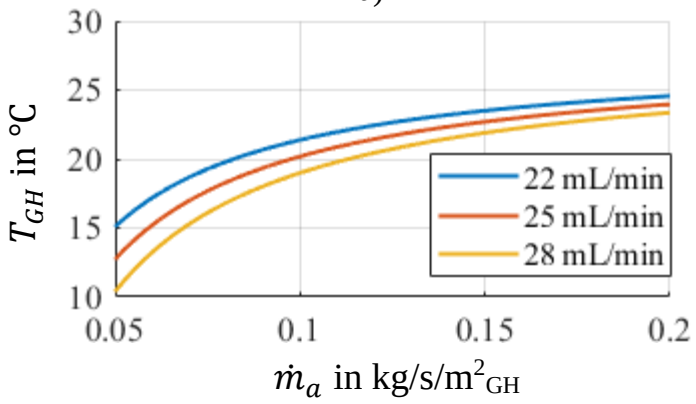
Figure 26 and
Figure 27 show that the footprint required by the evaporation chamber is mostly influenced by the droplet size. As larger droplets require longer EET, the footprint needs to be bigger to slow down the air stream and provide sufficient resident time. If the nozzles provide big droplets only, increasing the chamber height will also help keep the footprint small.

The following figures**, Figure 24** and **Figure 25**, show the influence $VPD_{GH,}$ T_1, RH_1, d_d and $\dot{m}_w$ have on the Estimated Evaporation Time (EET) of a droplet. Droplet diametrs of interest are equal to the predicted droplet size of the XA PR 050 nozzle, d_d = 25 to 35 µm. It can be seen that changes in inlet humidity and temperature have a minuscule effect on evaporation time. However, the droplet size drastically changes the duration. The markers show the exact air flow rate $\dot{m}_a$ needed to obtain VPD_{GH} = 1.0 kPa for different water flow rates. The EET calculated and shown in the figures are based on the corresponding T_2 and RH_2 values.

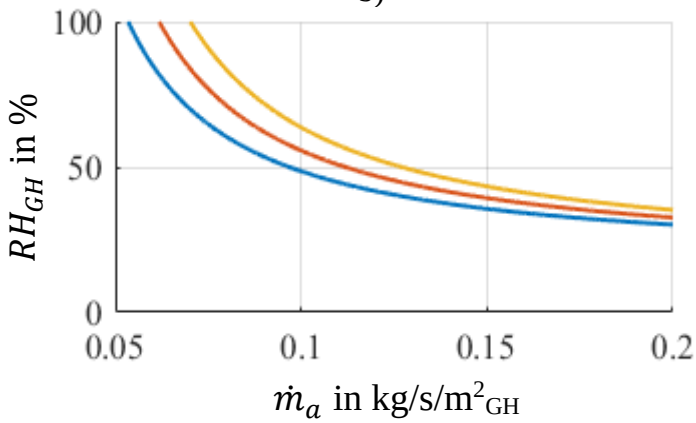
The following figures, **Figure 26** and **Figure 27** show the required evaporation chamber footprint in m^2 to keep 1 m^2 of greenhouse at a VPD_{GH} of 1.0 kPa. Droplet size has the biggest influence on EET. Droplet size, maximum chamber height H_{ECH} and inlet temperature T_1 are limiting factors. While a change in temperature influences the chamber size, the biggest effect can be observed by increasing the chamber height.



a)



b)



c)

Figure 20: VPD_{GH}, T_{GH}, RH_{GH} versus air flowrate for T_1 = 30 °C, RH_1 = 15 % and Q_{Sun} = 0.5 kW/m^2. a) influence water and air flowrate have on the VPD in the GH. The red line marks the necessary air flowrate $\dot{m}_a$ = 0.095 kg/s and water flowrate $\dot{m}_w$ = 25 mL/min required to result in a VPD of 1.0 kPa. Graph b) shows the expected temperature T_{GH} = 19.75 °C for $\dot{m}_w$ = 25 mL/min while Graph c) shows RH_{GH} = 58.9 % for a VPD of 1.0 kPa and $\dot{m}_w$ = 25 mL/min. As in Figure 18, temperature increases with decreasing water flowrate while the humidity decreases.

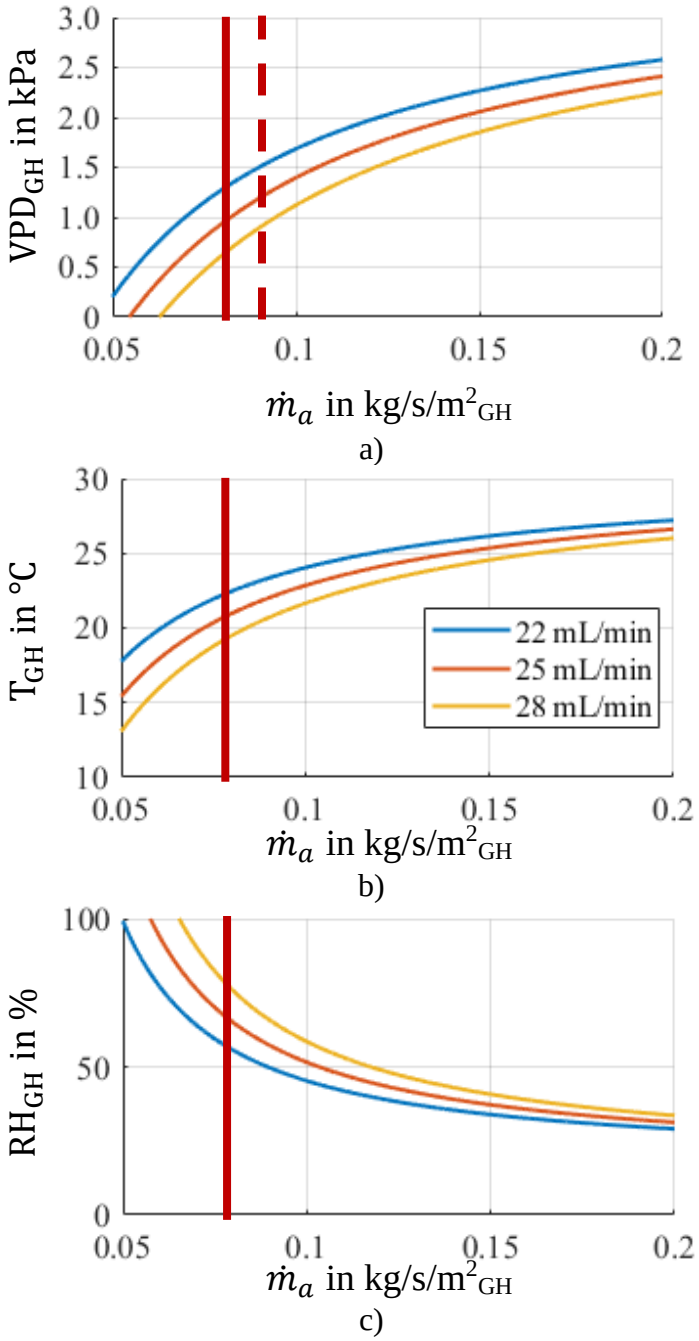


Figure 21: VPD_{GH}, T_{GH}, RH_{GH} versus air flowrate for T_1 = 33 °C, RH_1 = 15 % and Q_{Sun} = 0.5 kW/m^2. Graph a) illustrates the influence water and air flowrate have on VPD_{GH}. The red line marks the necessary air flowrate $\dot{m}_a$ = 0.082 kg/s and water flowrate $\dot{m}_w$ = 25 mL/min required to result in a VPD_{GH} of 1.0 kPa while the dotted red line shows the air flow required at lower T_1. Graph b) shows the expected temperature T_{GH} = 21.2 °C while Graph c) shows the relative humidity RH_{GH} = 63.2 % for a VPD_{GH} of 1.0 kPa and $\dot{m}_w$ = 25 mL/min. To continue operating at $\dot{m}_a$ = 0.095 kg/s and a VPD_{GH} = 1.0 kPa, higher water throughput is needed.

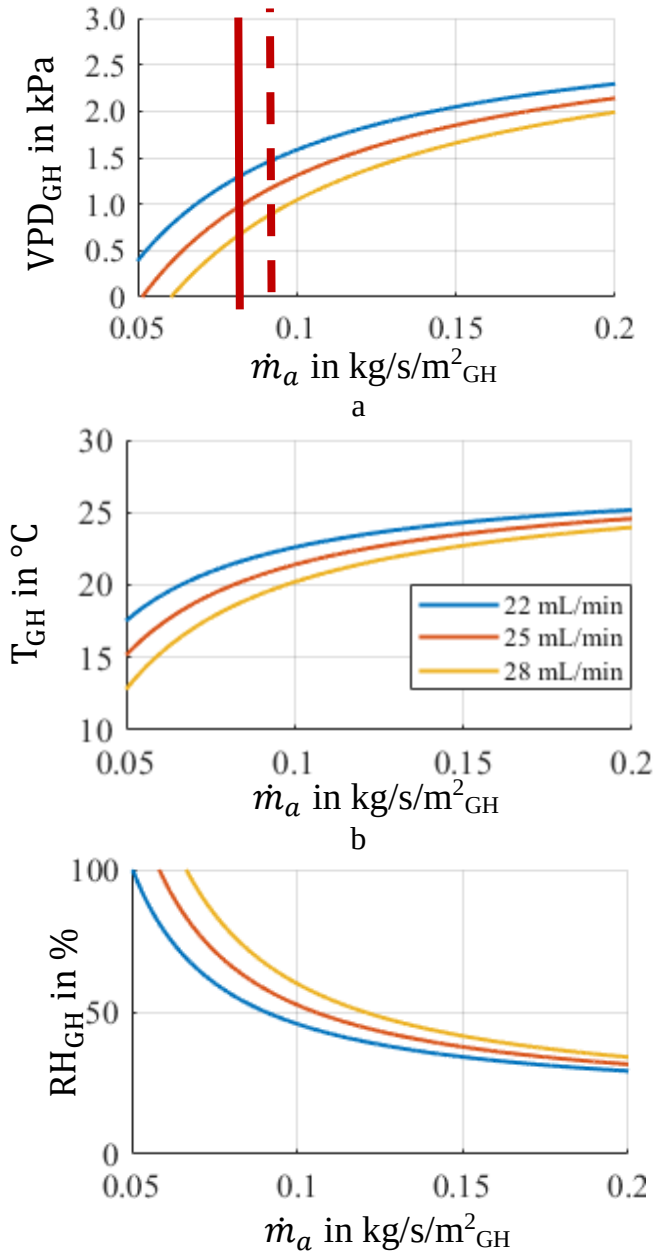


Figure 22: VPD_{GH}, T_{GH}, RH_{GH} versus air flowrate for T_1 = 30 °C, RH_1 = 15 % and Q_{Sun} = 0.75 kW/m^2. Graph a) illustrates the influence water and air flowrate have on the VPD_{GH}. The red line marks the necessary air flowrate $\dot{m}_a$ = 0.083 kg/s and water flowrate $\dot{m}_w$ = 25 mL/min required to result in a VPD_{GH} of 1.0 kPa while the dotted line shows the air flow required at lower Q_{Sun}. Graph b) shows the expected temperature T_{GH} = 20.1 °C while Graph c) shows the relative humidity RH_{GH} = 63.4 % for VPD_{GH} = 1.0 kPa and $\dot{m}_w$ = 25 mL/min. Higher heat rate increases temperature and decreases humidity. To compensate, lower air flowrate is needed to achieve chosen VPD_{GH} = 1.0 kPa..

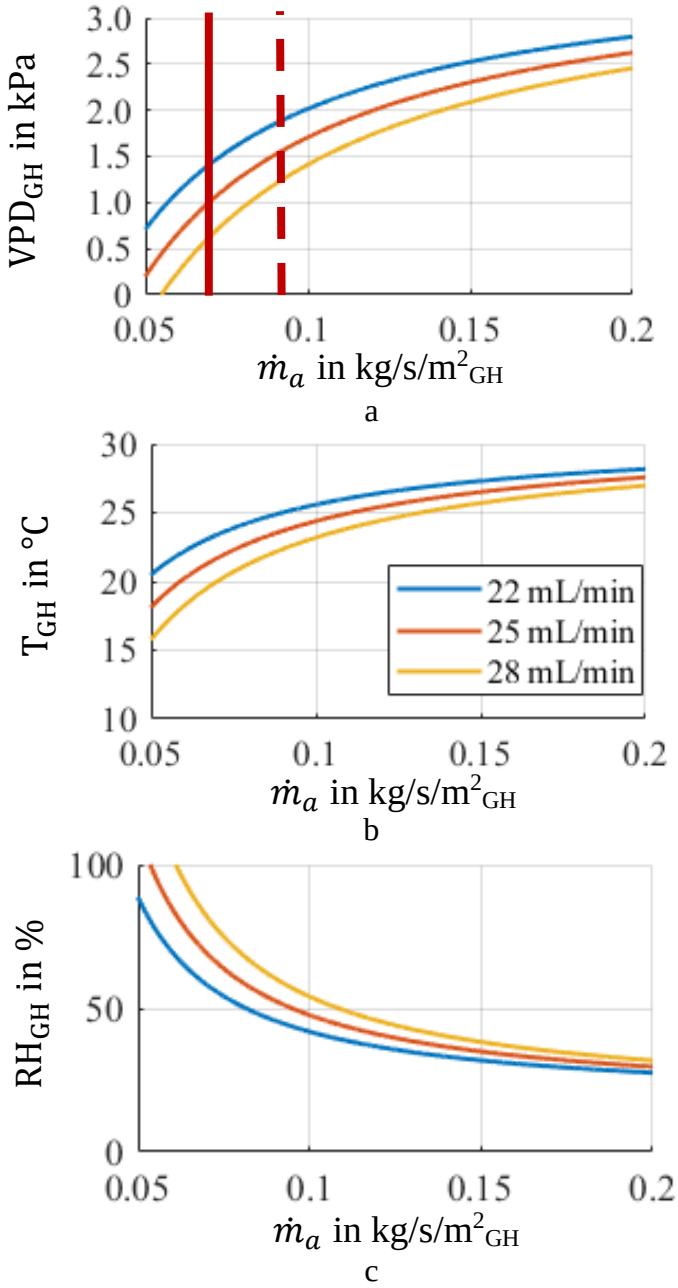


Figure 23: VPD_{GH}, T_{GH}, RH_{GH} versus air flowrate for T_1 = 33 °C, RH_1 = 15 % and Q_{Sun} = 0.75 kW/m^2. Graph a) illustrates the influence water and air flowrate have on the VPD_{GH}. The red line marks the necessary air flowrate $\dot{m}_a$ = 0.069 kg/s and water flowrate $\dot{m}_w$ = 25 mL/min required to result in a VPD of 1.0 kPa while the dotted line shows the air flow required at lower Q_{Sun} and lower T_1. Graph b) shows the expected temperature T_{GH} = 21.6 °C while Graph c) shows the relative humidity RH_{GH} = 69.75 % for VPD_{GH} = 1.0 kPa and $\dot{m}_w$ = 25 mL/min. Higher inlet temperature increases T_{GH} thus lowering necessary air flowrate at chosen VPD_{GH} = 1.0 kPa. Slow air flow leads to higher RH_2 which results in higher RH_{GH}.

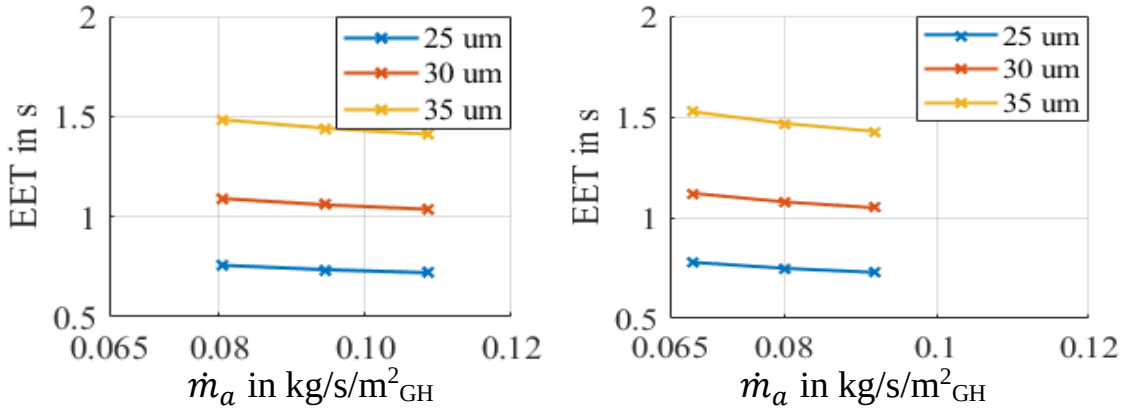


Figure 24: Estimated Evaporation Time (EET) for water droplet at RH_1 = 15 %, Q_{Sun} = 0.5 kW/m^2 and a) T_1 = 30 °C and b) T_1 = 33 °C. Markers indicate water flow rate $\dot{m}_w$ = 22 mL/min, 25 mL/min and 28 mL/min at air flow rates needed for VPD_{GH} = 1.0 kPa. EET calculated based on corresponding T_2 and RH_2 values.

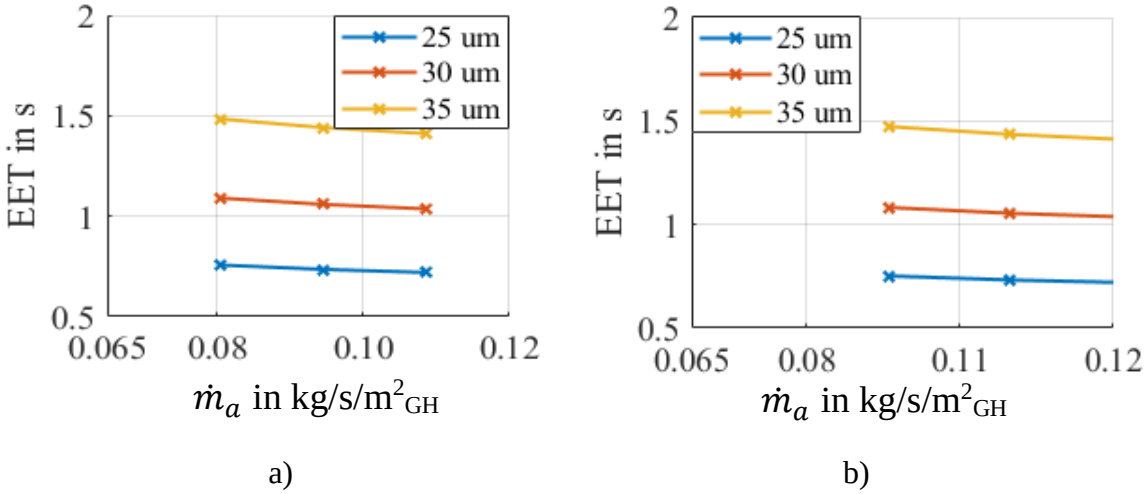


Figure 25: EET for water droplet at T_1 = 30 °C, Q_{Sun} = 0.5 kW/m^2 and a) RH_1 = 15 % and b) RH_1 = 20 %. Markers indicate water flow rate $\dot{m}_w$ = 22 mL/min, 25 mL/min and 28 mL/min at air flow rates corresponding to VPD_{GH} = 1.0 kPa.

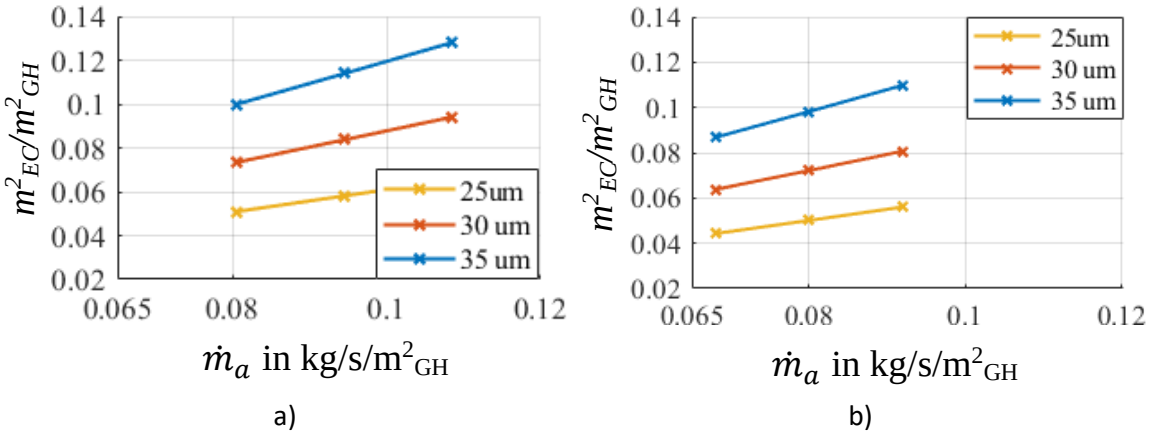


Figure 26: EC footprint for 1 m^2 of greenhouse with chamber height H_{ECH} = 1.5 m at VPD_{GH} = 1.0 kPa, RH_1 = 15 %, Q_{Sun} = 0.5 kW/m^2 and a) T_1 = 30 °C and b) T_1 = 33 °C. Markers indicate water flow rate $\dot{m}_w$ = 22 mL/min, 25 mL/min and 28 mL/min at air flow rates corresponding to VPD_{GH} = 1.0 kPa. Lower T_1 results in bigger footprint.

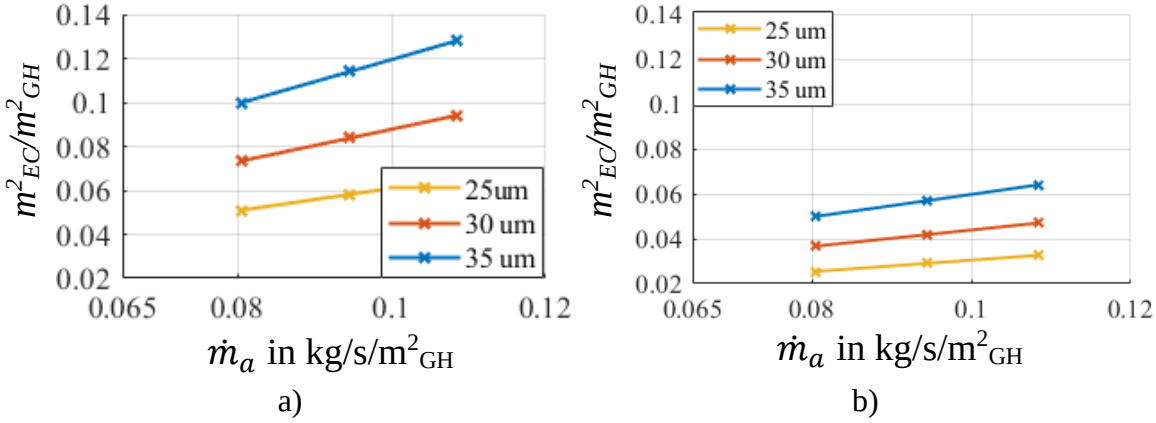


Figure 27: EC footprint for 1 m^2 of greenhouse with VPD_{GH} = 1.0 kPa, RH_1 = 15 %, Q_{Sun} = 0.5 kW/m^2, T_1 = 30 °C and a) H_{ECH} = 1.5 m and b) H_{ECH} = 2.5 m. Markers indicate water flow rate $\dot{m}_w$ = 22 mL/min, 25 mL/min and 28 mL/min at air flow rates corresponding to VPD_{GH} = 1.0 kPa. Higher chamber results in smaller footprint.

5. Experimental studies

An evaporation chamber setup has been experimentally tested. Experimental runs have been conducted with distilled water and 1 % (w/w) NaCl solution. For simplification purposes, only NaCl will be used in the experiments at a concentration of 1%. This is a slightly higher concentration than calculated in **Equation 5** based on the compounds in **Table 1** but will reduce errors in the fabrication of the liquid to a minimum and reduce the risk of breathing in toxic aerosols such as Selenium. Temperature and humidity are measured at various locations in the system for comparison to the model presented earlier.

If the system is operating as intended, salt will accumulate either on the blades and the dust chamber in the Louver Separator or on the collecting electrode of the ESP.

After each experiment, the Louver Separator or the Collecting Electrode will be removed from the system and rinsed with water. The leftover solution is heated to evaporate excess water thus leaving the NaCl accumulated during operation behind. By knowing the water flow rate, the collection efficiency can be calculated

5.1 Introduction of experiments

A schematic and photo of the experimental setup is shown in **Figure 28.** Contrary to the system design shown for application in

Figure 16, the air is pushed through the experimental setup rather than pulled. The ambient temperature of the laboratory T_{amb} = 21 °C is well below the planned operating temperature range of T_1 = 30 to 36 °C. Thus, a heater is needed to provide a sufficient inlet temperature T_1. The heater is installed at the bottom of the evaporation chamber and connected via an 8“ duct and a diffuser to ensure smooth flow behavior. To reduce the risk of fire, the fan was positioned ahead of the fan. In addition, the laboratory ceiling restricts the chamber design in height. With the diffuser and nozzle at the entrance and exit, the chamber itself can be no larger than 1 m in height. This fan configuration does increase the chance of leakage and will be addressed later on. C**hapter 5.1.1** and **Chapter 5.1.2** will elaborate on the experimental design and the sensors used to monitor the system.

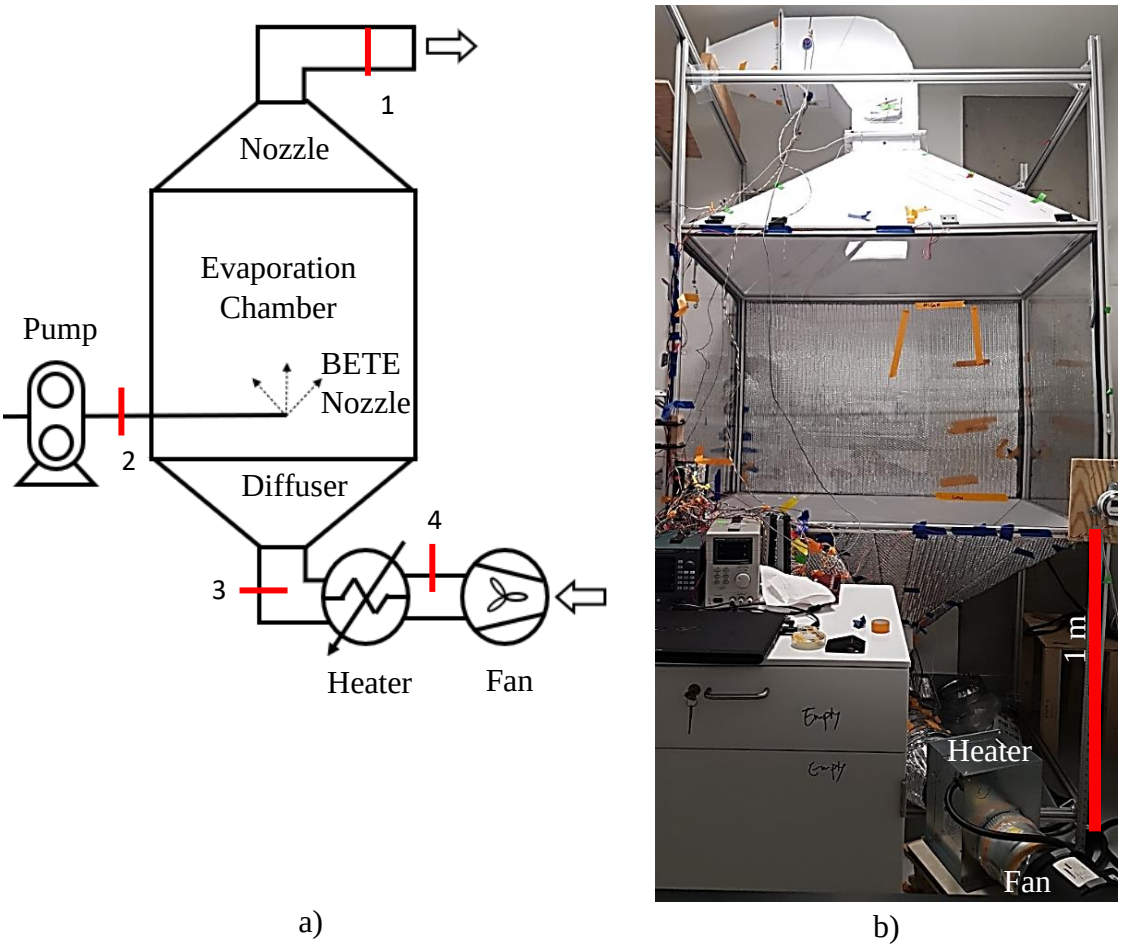
The first experiments were run on DI water to prevent clogging of the nozzle and aerosols at the outlet. The inlet temperature was chosen to be approximately T_1 = 33 °C as it reflects a mild summers day in the Central Valley. Successful runs show that the evaporation system can be used during early and late summers not, just during the hottest times of the year.

5.1.1 Experimental Design of Evaporation Chamber

The evaporation chamber has an aluminum extrusion frame. Such frames are easily modified and, with the attachment of casters, movable. The slots in the aluminum extrusion served as guides for 1/8” thick clear acrylic sheets. These sheets allow unobstructed observation of the processes taking place within the chamber. To make measuring airflow, temperature, and humidity easier, the inlet and outlet area were kept small compared to the 3 ft x 4 ft footprint of the chamber. An 8 inch diameter duct in combination with a diffuser

and nozzle manufactured from corrugated plastic, supply the chamber with air. To simulate hot ambient air, a heater was placed at the inlet. The heater used is produced by Neptronic and specified for output of 2 kW at 120 VAC. To provide a continuous air stream, a fan was installed in front of the heater. The fan is manufactured by VIVOSUN and offers variable speeds with a maximum air flow of 720 CFM. The atomizing nozzle mentioned previously is supplied with pressurized air from the lab and water using a Micro Dispensing Gear Pump CT3001F with pump head MG204 that allows accurate dispensing of liquid between 15-900 mL/min.

Figure 28a illustrates the configuration of setup and location of each component while **Figure 28b** shows a photo of the evaporation chamber in the laboratory.



a) b)

Figure 28: Evaporation chamber for experimental tests. a) Schematic of Evaporation Chamber. Red lines mark location of sensors. 1 indicates where the outlet humidity and temperature sensors are located. 2 shows the sensor for air and water pressure as well as water flowrate. At 3 the inlet humidity and temperature sensors are located. 4 shows the air flow sensor location. b) Chamber has a length of 4 ft and width of 3 ft. Total height of the chamber is equal to 0.95 m. With the diffuser and nozzle, the total height is 1.75 m. The red bar in the corner is equivalent to 1 m.

5.1.2 Sensors, Data Collection and Processing

The system behavior is monitored by a total of 20 sensors. There are four humidity and three temperature sensors located at the outlet and four humidity and three temperature sensors located at the inlet. These are spaced at 90° intervals around the periphery at these locations. The temperature sensors used are MA100GG103AN NTC Thermistors with a resistance of 10k at 25°C. The humidity sensors, HM1500LF, are produced by TE connectivity and specified for precise measurements between 10 to 95% relative humidity. However, as stated in the specification sheet, values beyond the operation range including condensation do not affect the reliability. The water flow is measured using Liquid Flow Sensor SLF3x by Sensirion. The sensor allows accurate measurement of up to ± 40 mL/min with a response time below 20 ms. The air and water pressure are measured using two compact pressure transducers, PX190, manufactured by OMEGA with an operating range of 0 to 75 PSI. The air flow at the inlet is measured using two MAFS Averaging Flow Sensors by Dwyer, spaced 4" apart and mounted perpendicular to another. **Table 6** gives an overview of the accuracy of each sensor. The data acquisition unit by LabJack is used for all sensors besides the SLF3x, as Sensirion provides their own data collection mechanism via a USB interface. Data collected by the LabJack is saved every 1.1 seconds during experiments while the SLF3x saves data every 5 ms. To account for fluctuations in the experiment and the different locations of the sensors, the values measured for temperature and relative humidity are averaged for each time recorded at both the outlet and inlet. The resulting data combined with the data collected by the pressure sensors and flow sensors is displayed graphically over the duration of the experiment.

Table 6: Sensor Specification

Sensors		Accuracy
Humidity	HM1500LF	± 3 %RH
Temperature	MA100GG103AN	± 0.1 °C
Air Flow Sensor	MAFS Averaging Flow Sensor	± 3 FS %
Water Flow Sensor	SFL3x	± 5 % or 0.05 mL/min whichever is bigger
Pressure Sensor	PX190	± 0.5 %

As can be seen in **Figure 30** , significant differences between the sensors are common, especially among the humidity sensors and to a lesser degree among the temperature sensors. Thus, the applicable error needs to account for this range. The difference between the lowest T or RH value to the highest is recorded, e.g. $\Delta RH = 10$ %. The total error reported is the sum of the listed accuracy in **Table 6** and half the difference, e.g. ± 8 % for RH readings with a 10% spread.

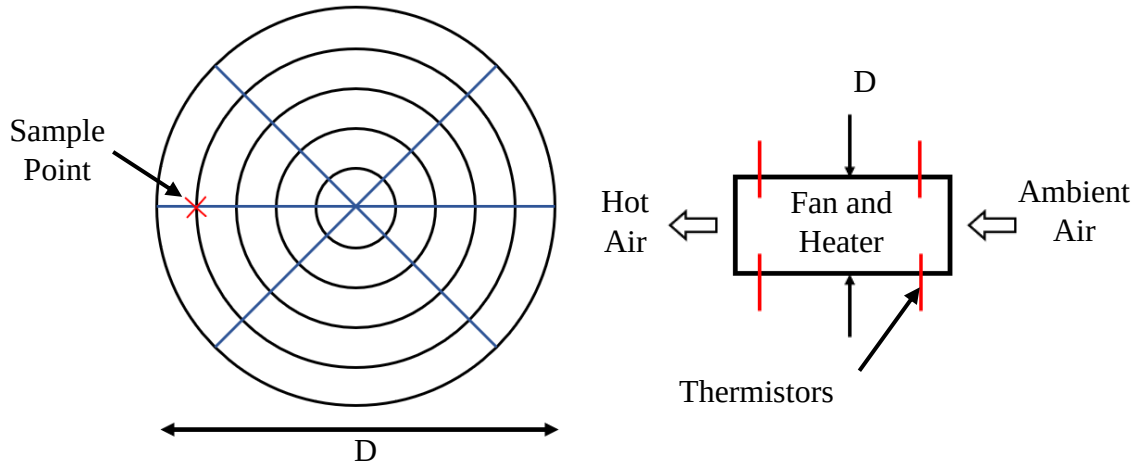
Uncertainty in air flow rate measurement is considered in a different manner. The accuracy provided by the company for the air flow sensor is over the full scale (FS) of operation which is equivalent to 45.7 m/s. This results in a potential error of ± 1.37 m/s. As this is more than half of the operating flow, and air flow has a major influence on the predicted outlet humidity and temperature, further measurements with a hot wire

anemometer and temperature sensors in combination with the heater were conducted to establish tighter bounds for uncertainty in flow rate.

The hot wire anemometer measured the flow rate in the duct following the pattern provided in **Figure 29a**. Each intersection between the radial and straight lines was a sample point. The flow rate was then averaged over the full inlet area and compared to the data collected by the MAFS flow sensor.

Taking advantage of energy conservation, temperature before and after the heater was also measured to determine the flowrate, see **Figure 29b**.

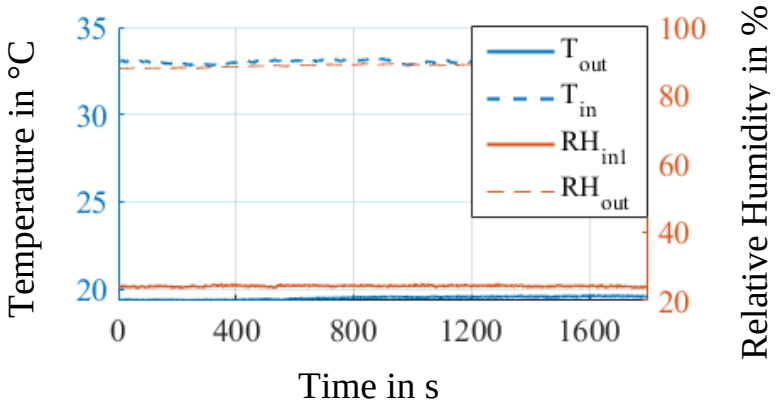
Both results showed, that at flowrates between 2 m/s to 3 m/s, an error of ± 3 % of the measured flowrate is appropriate.



a) b)

Figure 29: Additional air flow measurements. a) Sample pattern for hot wire anemometer b) Schematic of energy conservation measurement incldluing four thermistor, fan and the heater.

Figure 30 shows a typical data set for an evaporation experiment using distilled water. The data was recorded over 1800 s and sampled at 0.8 s. In the experiment, the nozzle was positioned in the diffuser, two inches below the chamber / diffuser interface. T_1 was held steady at 33 °C with an air flow rate of $\dot{m}_a$ = 0.086 kg/s. Pressurized air was supplied at 28 PSI while water was supplied at 23.43 PSI.



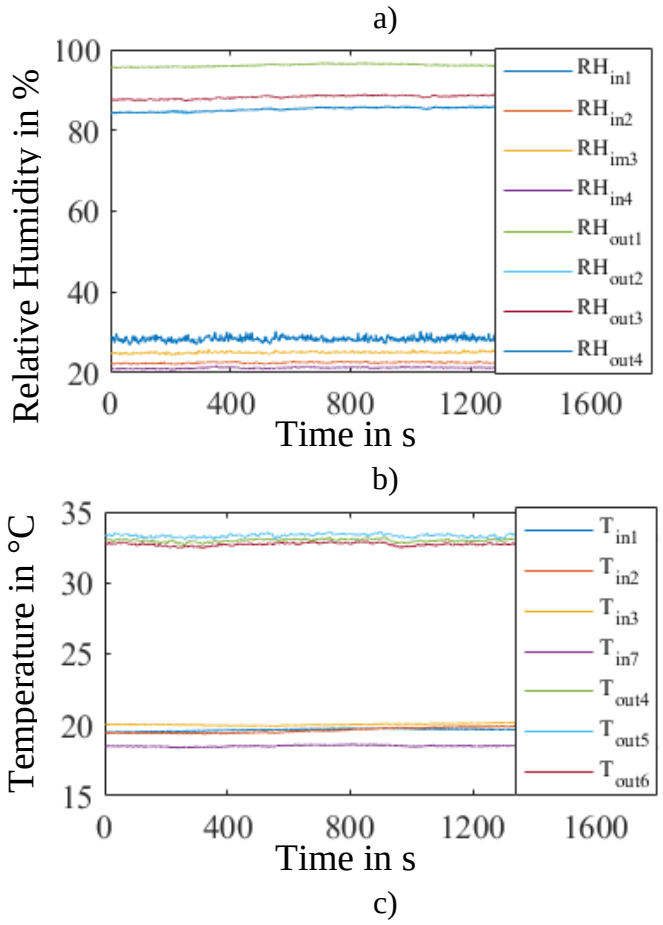


Figure 30: Data for distilled water evaporation test run. Total test duration was 1800 s at sample rate of 0.8 s. a) Average humidity and temperature at inlet and outlet b) Comparison of measurements for individual humidity sensors. Relative humidity sensors at the outlet show bigger deviation than sensors at the inlet. C) Comparison of measurements for individual temperature sensors. Sensors show relatively small range, but outlet shows most fluctuations. Water was provided at $\dot{m}_w$ = 24.86 mL/min and T_W = 22.4 °C.

5.1.3 Evaporation with Distilled Water

Table 7 shows data collected and averaged over 1800 s for three consecutive experiments. Experiment 1 was run with 27 PSI air pressure and consists of four data sets (120 min). Experiment 2 was run at 26 PSI air pressure and consists of six data sets (180 min), while Experiment 3 was run at 28 PSI air pressure and consist of four data sets (120 min). Not all water was evaporated during these experiments. The actual evaporated water flowrate was corrected by subtracting collected excess water from the overall input. The excess was collected beneath the diffuser in a small tray. No water accumulated at the outlet. Currently, the water excess is equivalent to 1.3 % of the measured water flow rate $\dot{m}_w$ in V1, 4.8 % in V2 and 2.1 %. Potential reasons and improvements are discussed in **Chapter 6**.

Table 7: Operating conditions during water evaporation test. Excess water at bottom of diffusor was used to calculate correct water evaporation rate. Duration of V1 was 120 min, duration of V2 was 180 min and duration of V3 was 120 min.

Version	T_1	RH_1	$\dot{m}_a$	$\dot{m}_{w,cor}$	Excess	T_2	RH_2	ω_2
	°C	%	kg/s	mL/min	mL/30 min	°C	%	$\frac{kg_w}{kg_{da}}$
1	33.03	15.26	0.0861	24.96	9.9	20.36	66.89	0.0099
2	33.07	22.08	0.0881	25.07	36.3	18.12	82.86	0.0108
3	33.05	23.57	0.0864	24.86	15.8	19.35	86.69	0.0127

Figure 31 shows the predicted humidity ratio values for the inlet conditions given in **Table 7** over an air flow rate range. As mentioned prior, error bars show the possible range of measured and predicted values based on the inlet and outlet conditions. The specific predicted humidity ratio at flowrate $\dot{m}_a$ from **Table 7** is marked with a dot. The x on the other hand marks the measured outlet data. In all three cases, the error bars overlap indicate relatively good agreement between model and experiments. Measured Experiment 1 and Experiment 3 values have a 4 % difference to the predicted values while Experiment 2 has a 8 % difference.

Possible reasons for discrepancies are further discussed in **Chapter 6**.

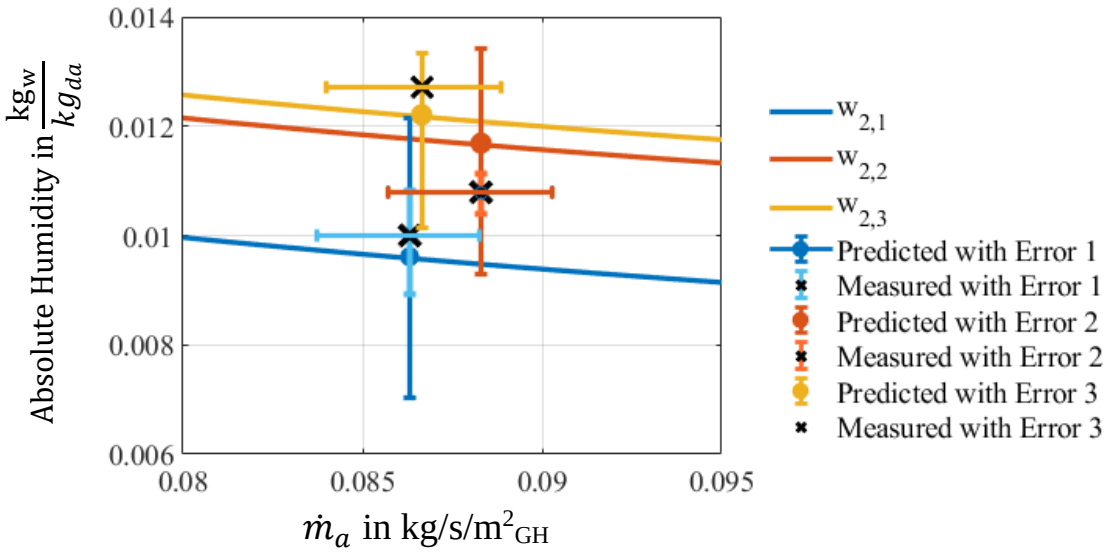


Figure 31: Comparison of Model and Experimental Data for Evaporation Chamber with Clean Water. The absolute humidity trend lines (blue, orange and yellow) were calculated based on the measured inlet temperature and humidity provided in **Table 7** for each experiment. Error bars around the trendlines indicate range of predicted outlet absolute

humidity while the error bar around the x show the potential absolute humidity range based on accuracy of the outlet sensors.

Knowing the absolute humidity and temperature at ② makes it possible to calculate the achievable VPD in the greenhouse based on the error margin of the sensors and Q_{Sun} (considered here for a range from 0.5 to 0.8 kW/m^2). **Table 8** shows the range of temperature and VPD predicted for a GH with a range of Q_{sun} values based on the conditions and sensor accuracy of Experiment 1 in **Table 7 .**VPD and T are a strong function of sun intensity. Depending on the size of Q_{Sun}, the VPD can be ideal for tomato growth in a greenhouse or far below or beyond the required climate. VPD control in particular depends on accurate measurement of relative humidity.

Table 8: Change in VPD_{GH} and T_{GH} over measured inlet data and range of Q_{Sun}. Positive error and negative error refer to the range of uncertainty for the experimental conditions. Temperature and VPD are strong functions of solar intensity.

	T_1	RH_1	$\dot{m}_a$	$\dot{m}_w$	VPD_{GH}			T_{GH}		
	°C	%	kg/s	mL/min	kPa			°C		
Q_{Sun} in kW/m^2					0.5	0.7	0.9	0.5	0.7	0.9
Measured	33.03	15.26	0.086	24.99	1.14	1.36	1.62	21.97	23.11	24.24
Positive Error	33.13	08.23	0.089	23.72	1.70	1.93	2.18	22.9	24.00	25.10
Negative Error	32.93	22.29	0.084	26.25	0.60	0.79	1.07	21.12	22.87	23.43

5.1.4 Evaporation with NaCl

Once evaporation chamber operation with distilled water was demonstrated, 1% NaCl (w/w) solution was used as feedwater. For these experiments, a separation chamber is attached to the existing system, see

Figure 14b. Thermodynamic data is collected following the procedure described in **Chapter 5.1.2** and shows behavior similar to pure water as discussed in **5.1.3**. The following **Table 9** shows the operating conditions during a test run. The experiment produced three data sets each 1800 s in duration. However, the total experiment duration includes an additional 30 min where water accumulated but the system had not yet fully reached steady state.

In the experiment, water was slowly accumulating in the separation chamber. A total of 92 mL of liquid was collected from the outlet air stream over the experiment duration, dropping the evaporated water flow rate from 25.24 to 24.56 mL/min. Excess water is equivalent to 2.7 % of the measured water flow.

Figure 32 shows the predicted humidity ratio values for the inlet conditions given in **Table 9** over an air flow rate range. As mentioned earlier, error bars show the possible range of measured and predicted values based on the inlet and outlet conditions. The

specific predicted humidity ratio at flowrate $\dot{m}_a$ from **Table 9** is marked with a dot. The X on the other hand marks the spot of the measured outlet data. The error bars indicate relatively good agreement between model and experiment with a difference between the measured experiment value X to the predicted value of 11 %. Possible reasons for discrepancies between them are discussed in **Chapter 6**.

Table 9: Operating Conditions during 1% (w/w) NaCl Solution Evaporation Test.

Version	T_1	RH_1	$\dot{m}_a$	$\dot{m}_{w,cor}$	Excess	T_2	RH_2	ω_2
	°C	%	kg/s	mL/min	mL/120 min	°C	%	$\frac{kg_w}{kg_{da}}$
1	33.03	15.26	0.0861	24.56	82	20.36	66.89	0.0099

To measure the salt collected by the system, the salt trapped in the separator had to be removed. This was accomplished by rinsing the louver-separator with DI water. **Figure** 33**a** shows the Louver Separator with remaining salt particles after the rinse. The diluted solution was then heated on a hot plate to evaporate the excess water, leaving the salt crystals behind. See **Figure 33b** where the drained water is slowly evaporating at a plate temperature of 120 °C. In total, 8.7 g of salt was collected. Knowing that the 1% NaCl (w/w) solution was supplied at 24.56 mL/min for a total duration of 120 minutes, leads to a total evaporated water volume of 2.95 L and potential salt deposit of 29.5 g. Thus, the collection efficiency in this experiment is 35 %.

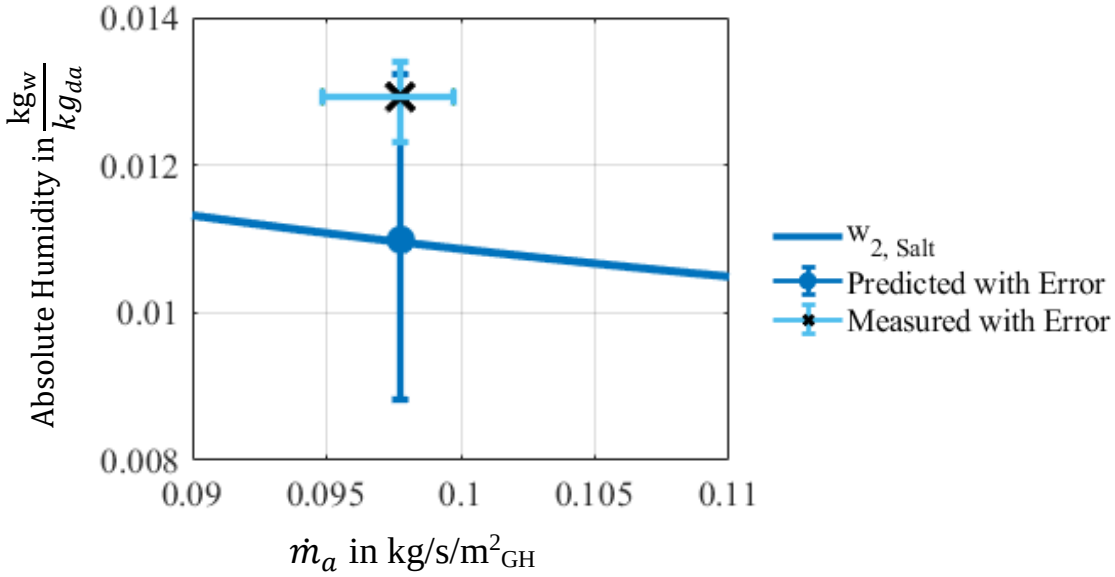


Figure 32: Comparison of Model and Experimental Data for Evaporation Chamber with 1% NaCl Solution. The absolute humidity trend lines (blue) was calculated based on the measured inlet temperature and humidity provided in **Table 9** for the experiment. Error

bars around the trendline indicate range of predicted outlet absolute humidity while the error bars around the x show the potential absolute humidity range based on accuracy of the outlet sensors. Collection efficiency of separation system is 35 %.



a) b)

Figure 33: Salt Recovery. a) Salt left in the Louver Separator after rinsing it with DI water. b) Water evaporation to remove liquid from salt crystals.

6. Overall System Function and Potential Improvements

6.1 Modelling

The model shows how VPD_{GH} changes based on a multitude of factors, e.g. RH_1, T_1, $Q_{Sun,}$ $\dot{m}_w$ and $\dot{m}_a$. Compare **Figure 20** to **Figure 23**. The biggest influence on VPD is inlet temperature T_1, followed by Q_{Sun}. As neither is adjustable in real life, water flow or air flow need to be adjusted to maintain a tolerable VPD in the greenhouse. As the objective is to use as much drainage water as possible and collect the particles for safe disposal, adjusting the water flow rate is recommended. This in turn allows for a constant air flowrate in the GH which provides a plant friendly environment all day long.

The analysis also showed that a better understanding of the inner workings of a greenhouse is needed. Currently, the range of solar intensity used in the model is too large (see **Table 8**). Depending on the measurement error and intensity of Q_{Sun}, the system could either be operating far beyond the acceptable range of VPD or exactly within it. Only a more accurate value for Q_{Sun} would allow predicting the exact operation range necessary.

Further, the model does not account for the moisture released by the plants. A closer collaboration with botanist and greenhouse agricultural researchers will be helpful in these respects.

Figure 24 to **Figure 27** show the influence droplet diameter has on the footprint of the evaporation chamber. Changes in inlet temperature T_1 and relative humidity RH_1 have a negligible effect on the duration of evaporation in comparison to droplet size. Currently, the droplet measures provided by the nozzle supplier (BETE) are only estimates due to the low operating air and water pressure. Running the system in the intended range will allow the accurate usage of the producer data base including droplet distribution. A better understanding of the droplet size will narrow the error margin in modelling. Moreover, installing temperature and relative humidity sensors throughout the chamber, rather than just the inlet and outlets, will improve the fidelity with which chamber temperature and humidity can be included in evaporation models. Rather than averaging T_1 and T_2 as well as RH_1 and RH_2, a more precise temperature and humidity distribution can be used.

6.2 DI Water Test

The test runs with water prove that the chamber is successful at evaporating water and generating cold and humid air at a rate predicted by the model of System I, see

Figure 31. The difference between predicted and measured value was as low as 3.9 % in V1 and all the error bars overlapped. However, **Figure 18** and **Figure 19** showed that the outlet humidity RH_2 and temperature T_2 are heavily influenced by water flowrate $\dot{m}_w$ and air flowrate $\dot{m}_a$. As both water and air flowrate have an error associated to them, it becomes difficult to operate at ideal conditions during experiments. The water flow supplied could exceed the actual needed flow rate due to an error in air flow readings. This leads to water accumulation and makes it necessary to adjust the actual water evaporation rate. Currently,

water excess ranges between 1.3 % for V1, to 4.8 % in V2. Excess water in V3 is equivalent to 2.1 %. Thus, full evaporation of the supplied water has not yet been achieved. The higher amount of excess water collected in V2 could also explain why the difference between predicted and measured w_2 is 8 %, considerably higher than the 3.9 % in V1 and V3.

Moreover, the chamber as built, is not airtight. Especially with positive air pressure, gaps are hard to seal, and the losses not accounted for by the model and airflow sensors. As T_2 and RH_2 are functions of $\dot{m}_a$, the predicted values based on the measured air flow rate could deviate further than initially assumed. This means future experiments require tighter monitoring of potential leaks.

The test runs with clean water all result in evaporation of water droplets before they reach the outlet. Excess water dripped down from the bottom part of the diffuser where water occasionally accumulated during operation due to droplet contact with the chamber walls. The amount of excess water is in direct correlation to the air pressure. Higher air pressure results in less excess water, see **Chapter 5.1.3**. V1 and V3 were operated at 27 PSI and 28 PSI respectively whereas V2 ran on 26 PSI. Less pressurized air leads to bigger water droplets which require higher EET. Those droplets are also heavier than the droplets produced at higher pressure in V1 and V3 and more likely to settle on the diffuser. Here, they merge with other droplets which increases their size till their weight overcomes gravity and the droplet runs down into the excess water tray.

Nevertheless, the data from **Table 8** confirm that the current settings are sufficient to provide cooling for a greenhouse to a satisfactory level 0.5 kPa < VPD_{GH} < 1.2 kPa, depending on solar intensity Q_{Sun}.

However, as soon as the separation system is attached, small water droplets appeared on the Louver Blades, signifying incomplete evaporation. One of the biggest changes introduced to the system through the Louver-Type Separator is the pressure drop. As a result, the air pattern within the chamber apparently changes. For the chamber without separator, turbulence appears to aid the evaporation process by mixing the droplets with the air. It also pushes some of the water onto the side panels of the chamber which could be collected after running down the diffuser. With the additional pressure drop, the new flow pattern no longer disturbs the mist, increasing the nozzle range, which reduces the residence time of the droplets in the warm chamber. Reducing the air pressure of the dual fluid nozzle does not help as the droplet size increases. Moreover, it is not possible to compensate with a higher water flowrate as it requires a higher air flowrate which in turn would accelerate the drops further. Additionally, the heater is limited by the maximum current capability of the variable transformer used to control power.

To address the excess water at the outlet, additional flow sensors need to be installed to monitor the air at the outlet. Also, the duration of the individual tests should be increased to reduce potential collection errors. The system could also benefit from running the nozzles at even higher air pressures. Fewer droplets would settle on the diffuser as the surface area to volume ratio would increase, rapidly decreasing EET. A slimmer and taller evaporation chamber would alleviate some of these issues, but the laboratory ceiling makes this modification impossible in the current setting. Purchasing a more powerful heater would also increase the air flow operating range and allow for simulation of extremely hot and dry summer months in the Central Valley. It would also make it possible to run airflow and water flow rates needed to achieve a VPD_{GH} of 1.0 kPa for multiple Q_{Sun} values.

6.3 NaCl Solution Test

The test runs confirmed that T_2 and RH_2 predicted by modeling are achievable with the separation chamber attached to the evaporation chamber, see **Figure 32.** However, contrary to the tests conducted with DI water, liquid slowly accumulates at the outlet alongside salt. This could explain why the measured value of w_2 has a difference of almost 12 % to the predicted values compared to a 4 % difference in the clean water run. Moreover, the added pressure drop by the separator might have increased the humidity readings or dropped the temperature of the sensors as cooler and moist air built up around the separator. Only 4" separate the sensor locations from the salt collection unit.

This test also confirmed the correlation between air pressure and excess water. Previous tests showed that the evaporation chamber produces less excess water the higher the nozzle pressure. Here, 30 PSI yielded excess water at 2.7 % of the measured water flow rate. The value is slightly higher than the 2.1 % in V3 at 28 PSI but it is important to realize that an increase in air pressure increases the range of the nozzle. This combined with the lack of turbulence, allows water to accumulate at the top and bottom. The 2.7 % not evaporated is still far lower than the 4.8 % in V2 at 26 PSI.

This also means that some percentage of the salt does not accumulate in the separation system but in the duct leading towards it. Dry particles will follow the air stream to the Louver Separator and settle in the dust chamber after initial impact with the blades. Wet air, however, will deposit salt on the inside walls of the system as well as the separation chamber. A total of 8.7 g of NaCl was recovered (35 % efficiency), confirming this theory.

As mentioned prior, the change in air dynamics is responsible for the excess water at the outlet. Droplets are no longer dispersed throughout the chamber but pushed towards the exit where they are not given enough time to fully evaporate. Slender and taller chambers would increase residence time but the ceiling height in the laboratory restricts changes in the vertical direction. An alternative to catch the remaining droplets of NaCl solution is necessary. One possibility is to take advantage salt crystallization. Rather than have the wet particles accumulate in the separator or the duct, a series of threads can be inserted into the air flow, not enough to introduce a substantial pressure drop but enough to catch the majority of the small droplets in flight. These threads will act as nucleation sites for the growth of crystals. Dry particles might attach as well but are more likely to follow the air stream upon collision with the strings as they have no liquid to bind to the thread. For maintenance, the threads can easily be removed and disposed of at landfills.

Before using this method, changing the Louver Separator for the Electrostatic Precipitator seems prudent. ESPs introduce a far smaller pressure drop to the system and should not overly influence the air flow pattern. However, to protect the electronics from moisture, the string method could be adapted as well.

7. Conclusion and Outlook

The experiments conducted with DI water and 1% NaCl solution confirmed that cooling a greenhouse with contaminated water is possible. 35 % of the supplied salt was successfully captured in the separation system. Moreover, measured data matched the predicted values for relevant thermodynamic variables – see overlapping error bars in

Figure 31 and

Figure 32**.** This increases confidence in the thermodynamic and evaporation model. As a result, an estimated evaporation chamber footprint can be predicted per 1 m^2 of GH. For the inlet conditions of the experiments, see **Table 7** and **Table 9**, the ratio varies between 0.04 to 0.1 m^2_{ECG}/m^2_{GH}. This means, a 100 m^2 GH can be cooled by a system that ranges from 4 to 10 m^2 at a chamber height of 1.5 to 2.5 m. The size marginally changes if different inlet conditions are provided and serve as guidance rather than absolute required size. More accurate information regarding the solar intensity will narrow the size range even further. Currently, the wide range of Q_{Sun} makes it hard to exclude certain operating conditions.

The work also confirmed that the surface area to volume ratio is crucial in evaporation. Higher air pressure and smaller droplets evaporate better. Less excess water was found in systems operating at high nozzle air pressure. Thus, the system needs to run on atomizers were the water flow and air flow rate can be adjusted independently. In the case of the XA PR 50 nozzle, this also increased the nozzle range. Hence a taller rather than wide ECH is needed

The experiments also showed that turbulence can be beneficial in evaporation chambers as they distribute the droplets and move them towards the hot air from the inlet. Droplets no longer gather at the end of the spray right before the outlet, and the residence time increases.

The models not only show the strong dependence on Q_{Sun} but also on $\dot{m}_a$. Air leaks needs to be avoided. Firstly, the drainage water is a complex mixture and can include toxic components that should not become airborne. Secondly, if cold air leaves the chamber prematurely, the cooling of the greenhouse will suffer and plant climate deteriorate. Lastly, an inaccurate $\dot{m}_a$ measurement will lead to non-fully evaporated drainage water (potentially in the separation system). This makes particle collection troublesome and could lead to particle deposits on the inside of the chamber. A negative air pressure in combination with tape or sealant should be favored. At worst for a negative pressure chamber, additional air is sucked into the system which would increase T_2 and decrease RH_2 but still guarantee full evaporation and dry particles in the separation system.

The upcoming summer months in the SJV can allow testing at operating conditions similar to the proposed operating range in the thesis. It may show if the theory holds true that XA PR 050 operates better in a slimmer but taller chamber.

The successful initial experiments show that the soil salinity issue and freshwater shortage could be significantly reduced in the future. Rather than dumping drainage water into retired fields or rivers, possibly deteriorating ground water, the system would replace fresh water purchased by the farmer with the run-off. Therefore, taking advantage of the scarce resource within, fresh water.

The system requires minimal updates to existing greenhouses as most are equipped with fans already for EVPs. These fans are powerful enough to pull the cold air from the evaporation chamber into the GH.

8. References

[1] California Department of Food and Agriculture, “California Agricultural Statistics Review 2017-2018,” 2018.

[2] T. B. Pathak, M. L. Maskey, J. A. Dahlberg, F. Kearns, K. M. Bali, and D. Zaccaria, “Climate change trends and impacts on California Agriculture: A detailed review,” *Agronomy*, vol. 8, no. 3, pp. 1–27, 2018, doi: 10.3390/agronomy8030025.

[3] D. Tilman, K. G. Cassman, P. A. Matson, R. Naylor, and S. Polasky, “Agricultural sustainability and intensive production practices,” *Nature*, vol. 418, no. 6898, pp. 671–677, Aug. 2002, doi: 10.1038/nature01014.

[4] G. Schoups *et al.*, “Sustainability of irrigated agriculture in the San Joaquin Valley, California,” *Proc. Natl. Acad. Sci. U. S. A.*, vol. 102, no. 43, pp. 15352–15356, 2005, doi: 10.1073/pnas.0507723102.

[5] A. L. Olmstead, P. W. Rhode, and J. Mcnamara, “A History of California Agriculture,” *Univ. Calif. Agric. Nat. Resour.*, vol. Giannini F, no. December, pp. 1–24, 2017.

[6] California Water Science Center, “California’s Central Valley.” [Online]. Available: https://ca.water.usgs.gov/projects/central-valley/about-central-valley.html.

[7] B. A. Cody and R. Johnson, “California Agricultural Production and Irrigated Water Use,” pp. 1–28, 2015.

[8] M. A. Maupin, J. F. Kenny, S. S. Hutson, J. K. Lovelace, N. L. Barber, and K. S. Linsey, *Estimated Use of Water in the United States in 2010*, vol. 1405, no. November. 2010.

[9] “The Strategic Plan, California Water Today,” *Calif. Water Balanc. by Water Year Data Table*, vol. 1, pp. 3–35, 2014.

[10] Bureau of Reclamation, “About Us - Fact Sheet.” [Online]. Available: https://www.usbr.gov/main/about/fact.html.

[11] DWR, “San Joaquin Valley Drainage Monitoring Program 2002,” *Calif. Dep. Water Resour.*, 2007.

[12] D. W. Ayers, R.S., Westcot, *Water quality for agriculture*, vol. 1, no. 1. 1989.

[13] G. Cismowski, W. Cooley, L. Grober, J. Martin, M. McCarthy, and R. Schnagl, “Salinity in the Central Valley,” 2006.

[14] G. S. Bañuelos and Z. Q. Lin, “Reuse of agricultural drainage water in central California: Phytosustainability in soil with high levels of salinity and toxic trace elements,” *Geol. Soc. Spec. Publ.*, vol. 266, pp. 79–88, 2006, doi: 10.1144/GSL.SP.2006.266.01.07.

[15] Water Education Foundation, “Salinity in the Central Valley: A Critical Problem.” [Online]. Available: https://www.watereducation.org/post/salinity-central-valley-critical-problem.

[16] C. A. Madramootoo, W. R. Johnston, and L. S. Willardson, *Management of agricultural drainage water quality: Water Report 13*. International Commission on Irrigation and Drainage, 1997.

[17] Water Education Foundation, “Land Retirement.” [Online]. Available: https://www.watereducation.org/aquapedia/land-retirement.

[18] K. Tanji, D. Davis, C. Hanson, A. Toto, R. Higashi, and C. Amrhein, “Evaporation ponds as a drainwater disposal management option,” *Irrig. Drain. Syst.*, vol. 16, no. 4, pp. 279–295, 2002, doi: 10.1023/A:1024877630332.

[19] J. W. Bartok, “Natural Ventilation in Greenhouses,” *The Centre for Agriculture, Food and Environment*, 2013. [Online]. Available: https://ag.umass.edu/greenhouse-floriculture/fact-sheets/natural-ventilation-in-greenhouses.

[20] V. P. Sethi and S. K. Sharma, “Survey of cooling technologies for worldwide agricultural greenhouse applications,” *Sol. Energy*, vol. 81, no. 12, pp. 1447–1459, Dec. 2007, doi: 10.1016/j.solener.2007.03.004.

[21] D. H. Willits, “Cooling fan-ventilated greenhouses: A modelling study,” *Biosyst. Eng.*, vol. 84, no. 3, pp. 315–329, 2003, doi: 10.1016/S1537-5110(02)00270-2.

[22] H. A. Ahemd, A. A. Al-faraj, and A. M. Abdel-ghany, “Shading greenhouses to improve the microclimate , energy and water saving in hot regions : A review,” *Sci. Hortic. (Amsterdam).*, vol. 201, pp. 36–45, 2016, doi: 10.1016/j.scienta.2016.01.030.

[23] M. K. Ghosal and G. N. Tiwari, “Modeling and parametric studies for thermal performanceof an earth to air heat exchanger integratedwith a greenhouse.pdf,” *Energy Convers. Manag.*, vol. 47, no. 13–14, pp. 1779–1798, 2006.

[24] R. Bucklin, R. W. Henley, D. B. McConnell, Florida Cooperative Extension Service, and Palmm Project, “Fan and Pad Greenhouse Evaporative Cooling Systems 1,” *Water*, no. January 2004, pp. 1–7, 2004.

[25] R. O. Williams, A. B. Watts, and D. A. Miller, *Formulating Poorly Water Soluble Drugs*. 2012.

[26] N. Ashgriz, *Handbook of Atomization and Sprays*. 2011.

[27] K. Lüchow and C. Von Zabeltitz, “Investigation of a spray cooling system in a plastic-film greenhouse,” *J. Agric. Eng. Res.*, vol. 52, no. C, pp. 1–10, 1992, doi: 10.1016/0021-8634(92)80046-U.

[28] T. Akinaga, S. C. Generalis, C. Paton, O. N. Igobo, and P. A. Davies, “Brine utilisation for cooling and salt production in wind-driven seawater greenhouses: Design and modelling,” *Desalination*, vol. 426, no. February 2017, pp. 135–154, 2018, doi: 10.1016/j.desal.2017.10.025.

[29] T. Akinaga, S. C. Generalis, C. Paton, O. N. Igobo, and P. A. Davies, “Brine utilisation for cooling and salt production in wind-driven seawater greenhouses: Design and modelling,” *Desalination*, vol. 426, pp. 135–154, Jan. 2018, doi: 10.1016/j.desal.2017.10.025.

[30] A. Ahmadinik, A. Rahimikhoob, and S. Aliniaeifard, “Water use efficiency in novel integrated system of greenhouse and saltwater evaporative pond,” *Desalination*, vol. 496, Dec. 2020, doi: 10.1016/j.desal.2020.114698.

[31] A. M. Al-Ismaili and H. Jayasuriya, “Seawater greenhouse in Oman: A sustainable technique for freshwater conservation and production,” *Renew. Sustain. Energy Rev.*, vol.

54, pp. 653–664, Feb. 2016, doi: 10.1016/j.rser.2015.10.016.

[32] M. H. El-Awady, H. H. El-Ghetany, and M. A. Latif, “Experimental Investigation of an Integrated Solar Green House for Water Desalination, Plantation and Wastewater Treatment in Remote Arid Egyptian Communities,” *Energy Procedia*, vol. 50, pp. 520–527, Jan. 2014, doi: 10.1016/j.egypro.2014.06.063.

[33] H. Sadafi, I. Jahn, and K. Hooman, “Heat Transfer in Saline Water Evaporative Cooling,” *Heat Transf. Eng.*, vol. 40, no. 5–6, pp. 429–436, 2019, doi: 10.1080/01457632.2018.1432023.

[34] K. Cal and K. Sollohub, “Spray Drying Technique. I: Hardware and Process Parameters,” *J. Pharm. Sci.*, vol. 99, no. 2, pp. 575–586, Feb. 2010, doi: 10.1002/jps.21886.

[35] A. Ogawa, *Separation of particles from air and gases. Volume 1*. 1984.

[36] ENVIRONMENTAL PROTECTION AGENCY, *Control of Particulate Matter Emissions Student Manual Chapter 5*. .

[37] K. Sutherland and G. Chase, *Filters and Filtration Handbook*, 5th ed. 2008.

[38] J. B. Sim, U. H. Yeo, G. H. Jung, S. B. Park, G. N. Bae, and S. J. Yook, “Enhancement of louver dust collector efficiency using modified dust container,” *Powder Technol.*, vol. 325, pp. 69–77, Feb. 2018, doi: 10.1016/j.powtec.2017.10.047.

[39] J. L. Smith and M. J. Goglia, “The mechanism of separation in the louver-type dust separator,” *J. Air Pollut. Control Assoc.*, vol. 5, no. 1, pp. 51–62, 1955, doi: 10.1080/00966665.1955.10467685.

[40] G. O. Musgrove, M. D. Barringer, K. A. Thole, E. Grover, and J. Barker, “Computational design of a louver particle separator for gas turbine engines,” *Proc. ASME Turbo Expo*, vol. 3, no. PART B, pp. 1313–1323, 2009, doi: 10.1115/GT2009-60199.

[41] ENVIRONMENTAL PROTECTION AGENCY, *Control of Particulate Matter Emissions Student Manual Chapter 9*. .

[42] A. Mizuno, “Electrostatic precipitation,” *IEEE Trans. Dielectr. Electr. Insul.*, vol. 7, no. 5, pp. 615–624, 2000, doi: 10.1109/94.879357.

[43] M. Chandra, J. Sarat, and H. Sekhar, “Effect of Particle Size on Collection Efficiency of ESP and RABH : A Case Study,” *Aerosol Sci. Eng.*, no. 0123456789, 2019, doi: 10.1007/s41810-019-00045-2.

[44] Y. Zhuang, Y. J. Kim, T. G. Lee, and P. Biswas, “Experimental and theoretical studies of ultra-fine particle behavior in electrostatic precipitators,” *J. Electrostat.*, vol. 48, no. 3–4, pp. 245–260, 2000, doi: 10.1016/S0304-3886(99)00072-8.

[45] R. Zevenhoven and P. Kilpinen, *Control of pollutants in flue gases and fuel gases*, no. June. 2001.

[46] “Fan Power Consumption.” [Online]. Available: https://www.engineeringtoolbox.com/fans-efficiency-power-consumption-d_197.html.

[47] R. R. Shamshiri, J. W. Jones, K. R. Thorp, D. Ahmad, H. C. Man, and S. Taheri, “Review of optimum temperature, humidity, and vapour pressure deficit for microclimate

evaluation and control in greenhouse cultivation of tomato: A review," *Int. Agrophysics*, vol. 32, no. 2, pp. 287–302, 2018, doi: 10.1515/intag-2017-0005.

[48] H. J. Holterman, *Kinetics and evaporation of water drops in air*, no. July. 2003.

[49] M. H. Sadafi, I. Jahn, A. B. Stilgoe, and K. Hooman, "A theoretical model with experimental verification for heat and mass transfer of saline water droplets," *Int. J. Heat Mass Transf.*, vol. 81, pp. 1–9, 2015, doi: 10.1016/j.ijheatmasstransfer.2014.10.005.